In Vitro Assessment of Putative PD-1/PD-L1 Inhibitors: Suggestions of an Alternative Mode of Action

Derek J. Blevins, Ronan Hanley, Trevor Bolduc, David A. Powell, Michael Gignac, Kayleigh Walker, Mark D. Carr, Fraser Hof, and Jeremy E. Wulff

2019

In Vitro Assessment of Putative PD-1/PD-L1 Inhibitors: Suggestions of an Alternative Mode of Action.

Derek J. Blevins,† Ronan Hanley,† Trevor Bolduc,† David A. Powell,‡ Michael Gignac,† Kayleigh Walker,§ Mark D. Carr,§ Fraser Hof,† and Jeremy E. Wulff *†

† Department of Chemistry, University of Victoria, PO Box 3065 STN CSC, Victoria, British Columbia, Canada, V8W 3V6

‡ Inception Sciences Canada, 210-887 Great Northern Way, Vancouver, British Columbia, Canada, V5T 4T5

§ Leicester Institute of Structural and Chemical Biology, University of Leicester, Leicester, United Kingdom

KEYWORDS: PD-1, PD-L1, protein–protein interaction inhibitors, SPR.

ABSTRACT: The programmed cell death protein 1 (PD-1) signaling axis is among the most important therapeutic targets in modern oncology. Aurigene Discovery Technologies Ltd. (Aurigene) has patented a series of peptidomimetic small molecules derived from the PD-1 protein sequence for use in targeting the interaction between PD-1 and its ligand, PD-L1. We evaluated three of Aurigene's most potent compounds in SPR binding assays. Our results showed that these compounds – each of which is known to be potently effective in a splenocyte recovery assay – do not directly inhibit the PD-1/PD-L1 interaction, nor do they appear to bind to either of the constituent proteins, indicating that another mechanism is at play. As a result of these studies and upon consideration of structural features within the PD-1/PD-L1 complex, we hypothesize that the Aurigene molecules may interact with a currently unknown protein capable of regulating the PD-1 axis.

Programmed cell death protein 1 (PD-1) and its ligand (PD-L1) are transmembrane immunosuppressive checkpoint proteins.[1] PD-1 is expressed on activated T cells, and PD-L1 is expressed on somatic tissue and antigen-presenting cells.[2,3] The binding interaction between PD-1 and PD-L1 causes a down-regulation of T cell proliferative gene expression, thus disrupting cytotoxic activity. Certain aggressive cancers, such as pancreatic cancer, breast cancers, and non-small lung carcinomas have evolved to overexpress PD-L1 as a means of immune evasion.[3,4] In these cases, PD-L1 expresses constitutively, allowing the tumor to masquerade as immune privileged tissue and evade detection.[5–8] Overexpression of PD-L1 is therefore a strong prognostic biomarker in oncology.[2–12]

Table 1. A List of Current FDA-approved Immunotherapeutics that Block the PD-1/PD-L1 interaction.[13–17]

name	company	target	FDA approval year
nivolumab	Bristol-Myers Squibb	PD-1	2014
pembrolizumab	Merck	PD-1	2014
atezolizumab	Genentech/Roche	PD-L1	2016
avelumab	Merck	PD-L1	2017
durvalumab	AstraZeneca	PD-L1	2017
cemiplimab	Regeneron/Sanofi	PD-1	2018

Pharmaceutical companies have sought to develop modulators for the PD-1/PD-L1 interaction to recover lymphocyte activity. Current treatments are antibody-based therapies targeting either PD-1 or PD-L1 (Table 1). Despite the remarkable therapeutic success of these antibodies,[13,17–25] there are considerable drawbacks such as poor bioavailability, immunogenicity, and the high cost of large-scale production.[13,26,27] Small molecule inhibitors have the potential to overcome these obstacles, and multiple research groups are pursuing this objective.[28–30] However, there are currently no FDA-approved small molecule inhibitors capable of blocking the PD-1/PD-L1 interaction.[31,32]

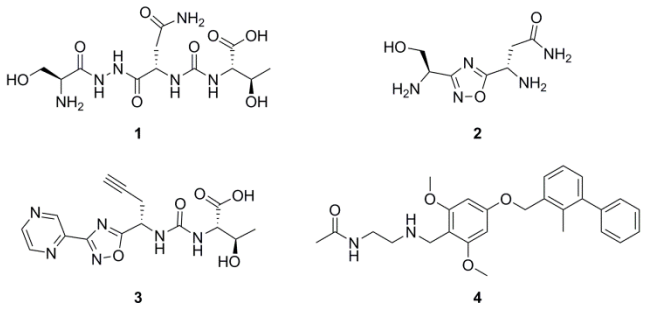

Figure 1. Compounds used for the present study. Compounds **1**–**3** are patented immunomodulators from Aurigene, hypothesized to disrupt the PD-1/PD-L1 interaction. Compound **4** is a known inhibitor developed by Bristol-Myers Squibb, employed here as a positive control.

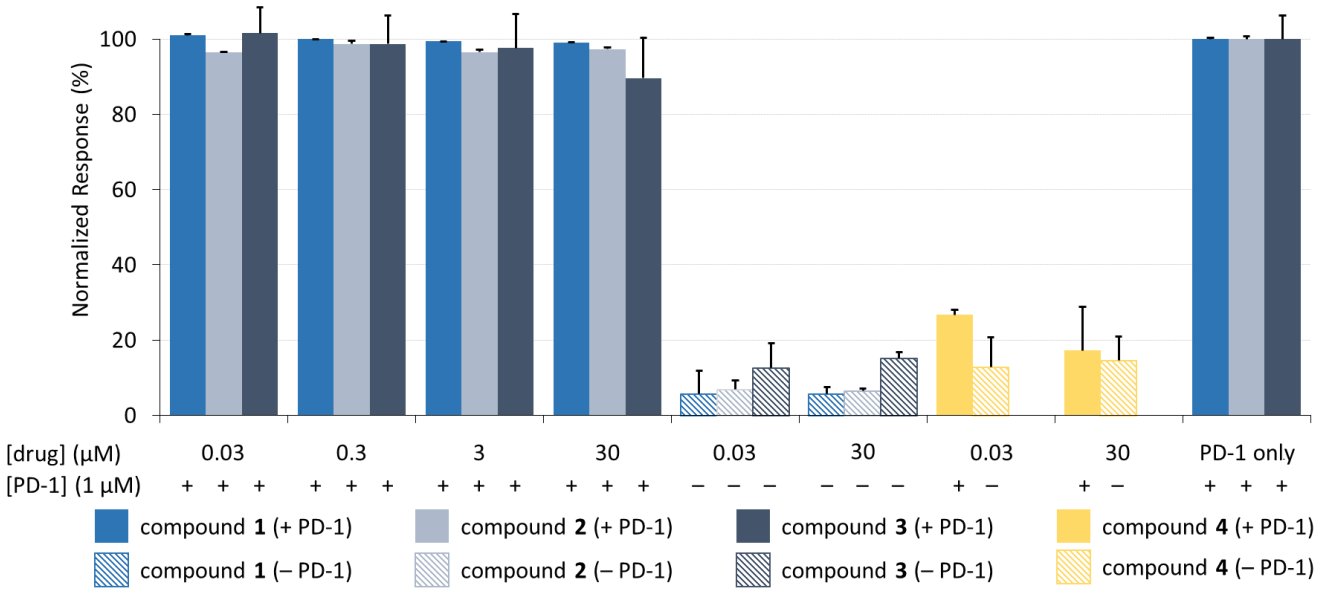

Figure 2. The Aurigene compounds (**1**–**3**) show no inhibition between 30 nM and 30 μM for PD-1 flowing over PD-L1. Soluble PD-1 was flowed across surface-bound PD-L1 with and without test compounds at varying concentrations. The response is normalized to the control protein interaction (PD-1 only). Responses were measured in triplicate and error bars represent standard deviation.

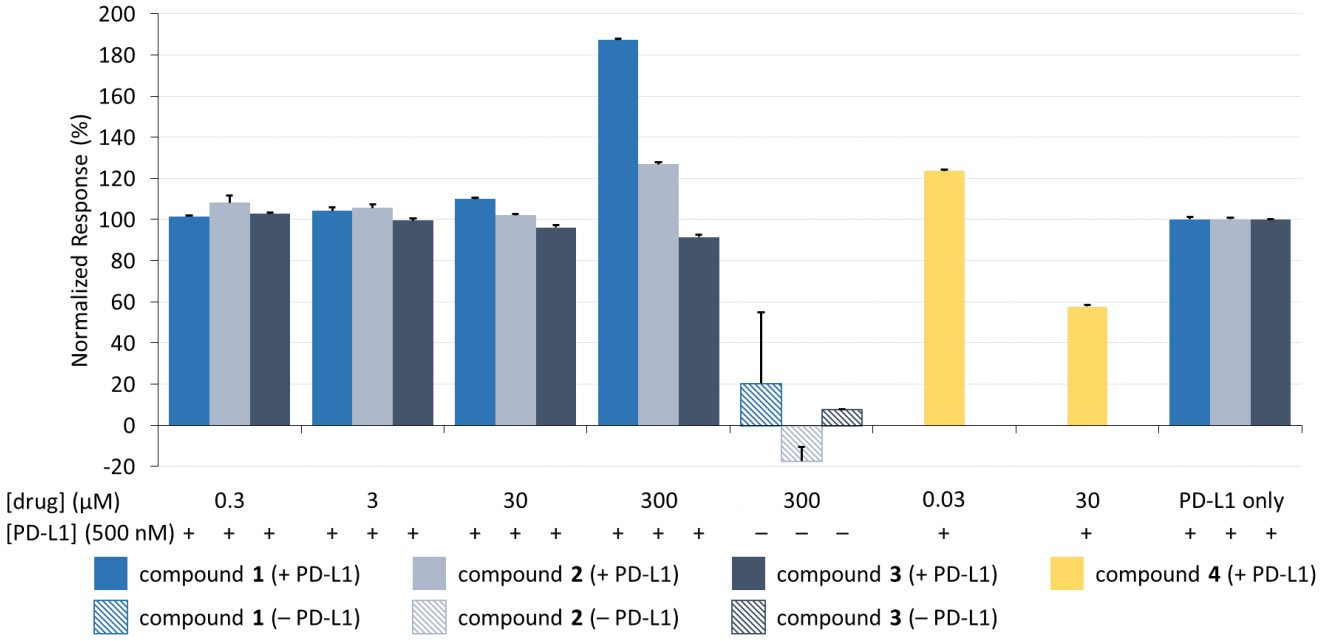

Figure 3. The Aurigene compounds (**1**–**3**) show no inhibition between 300 nM and 300 μM for PD-L1 flowing over PD-1. Soluble PD-L1 was flowed across surface-bound PD-1 with and without test compounds at varying concentrations. The response is normalized to the control protein interaction (PD-L1 only). Responses were measured in triplicate and error bars represent standard deviation.

Aurigene has an extensive patent portfolio of peptides and peptidomimetic small molecules that mimic various regions of the PD-1 protein sequence. The most promising peptidomimetic compounds are reported to exhibit nanomolar potency in a phenotypic cell-based splenocyte recovery assay that Aurigene uses to scout for PD-1/PD-L1 inhibitors.[33–37] However, no direct protein binding experiments have been reported for this family of small molecules. We selected three of the most promising compounds (Figure 1) from three recent patents[35–37] and aimed to characterize them using new surface plasmon resonance (SPR)-based methods. Each test compound was chosen with an eye toward maximizing both potency and drug-like properties, while optimally representing the compounds claimed within each patent.

Using SPR, we developed inhibition assays to detect how binding between the extracellular domain of PD-1 and the extracellular domain of PD-L1 is affected in the presence of the Aurigene compounds (refer to Figures S1 and S2 in the Supporting Information for sensorgrams showing PD-1/PD-L1 binding). In our first inhibition assay (Figure 2), biotinylated PD-L1 was adsorbed on a

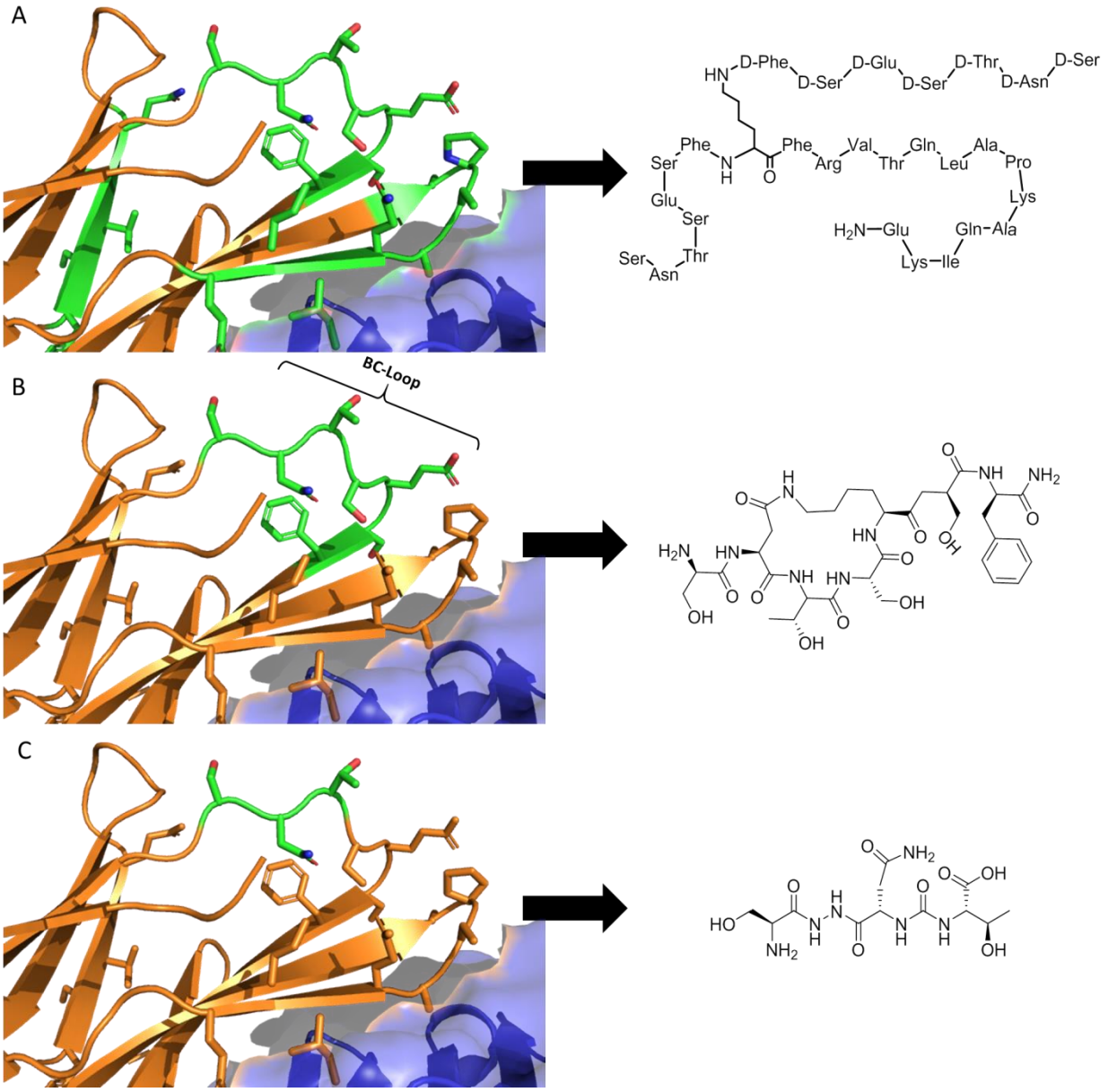

Figure 4. The binding interface between PD-1 and PD-L1, together with an illustration of the discovery process leading to Aurigene's lead compounds. PD-1 and PD-L1 are shown in cartoon representation (orange) and surface representation (blue) respectively. Residues highlighted in sticks are the residues the patent compounds are derived from. A) Left: Residues (57–63, 95–99, 127–136) of the PD-1 protein. Right: Patented peptide derived as a structural analogue to the region. B) Left: Residues (57–63) of the PD-1 protein. Right: Patented macrocyclic compound derived as a structural analogue to the region. C) Left: Residues (57–59) of the PD-1 protein. Right: Small molecule peptidomimetic derived as a structural analogue to the region.

streptavidin-coated gold chip (SA chip). Varied concentrations (ranging from 30 nM – 30 μM concentrations) of Aurigene compounds **1**–**3** were titrated over a flow cell in the presence of recombinant soluble PD-1 (corresponding to residues P34–E150 of the native protein).

The binding responses were normalized to PD-1 binding to PD-L1 (control). Compounds acting as inhibitors of the PD-1/PD-L1 interaction would decrease the binding response relative to the control. To validate the assay, we used a known PD-1/PD-L1 inhibitor from Bristol-Myers Squibb as a positive control (compound **4**, data shown in yellow).[29] Previous studies have shown that compound **4** induces a dimerization of the PD-L1 proteins, preventing PD-1 from binding.[38–40] As expected, compound **4** showed effective in vitro inhibition at both low concentrations (30 nM) and high concentrations (30 μM). For titration data associated with **4**, see Figures S3 and S4.

When compounds **1**–**3** were tested in this assay, we observed no change in binding between the two proteins (Figure 2). Moreover, in the absence of PD-1 protein (data shown in hashed columns) the Aurigene compounds **1**–**3** also elicited little signal variance between 30 nM and 30 μM, suggesting that there is no directly observable binding to PD-L1. While a very small signal was likewise observed for **4** in the absence of PD-1, this is consistent with the known 2:1 binding mode between PD-L1 and compound **4**.[38] Such

behavior would effectively double the molecular weight of the receptor (since **4** binds to a PD-L1 homodimer, rather than to monomeric PD-L1), while reducing the density of receptor on the surface of the chip (since not all surface-bound proteins would be able to homodimerize). The result would be very weak signal, since SPR response is proportional to both the ratios of the molecular weights of the two interacting species, and to the immobilization density.

We repeated the inhibition experiment, this time attaching biotinylated PD-1 to the gold surface and flowing recombinant PD-L1 protein (corresponding to residues A18-T239, chosen to represent both extracellular domains of the native protein) across the chip along with various concentrations of **1**–**4** (Figure 3). This type of reciprocal binding assay serves as an important control for binding artefacts in SPR experiments. Once again, the positive control molecule (**4**) was observed to inhibit the interaction (data shown in yellow), although in this case higher concentrations of **4** were required because of the high concentration of PD-L1 required in the experiment. These data provide additional support for the earlier study determining PD-L1 as the biological target for compound **4**.[39]

As in the previous assay, however, the Aurigene compounds **1**–**3** showed no inhibition of the PD-1/PD-L1 interaction (Figure 3), nor did they appear to elicit any statistically significant binding to adsorbed PD-1. At very high concentrations (300 μM), Aurigene compounds **1** and **2** gave an increase in SPR response (i.e. negative inhibition), but this is likely due either to molecules nonspecifically adsorbing to the attached protein or else to compound precipitation. The same results were observed in our assay for soluble PD-1 flowed over another adsorbed binding partner, PD-L2 (Figure S6). Compound **4** was also shown to not inhibit the PD-1/PD-L2 interaction and showed no sign of binding directly to PD-L2, highlighting the specificity of the BMS compound.

Seeking confirmation of these results in an orthogonal assay type, we also briefly explored the function of compound **1** in a commercial ELISA assay for PD-1/PD-L1 inhibitors (Figure S8). Once again, however, we saw no significant inhibitory activity. Positive controls (including compound **4** and two related inhibitors from Bristol-Myers-Squibb, as well as a known antibody inhibitor) all worked as expected, once again validating the assay.

Aurigene characterized the efficacy of their lead compounds using a phenotypic cell-based assay built around splenocyte recovery as a proxy for immune activation. Compounds **1**–**3** triggered high recovery in this experiment (68%, 93%, and 92%, respectively, relative to an uninhibited positive control) at 100 nM.[35–37] The limited experimental data in Aurigene's patents (including controls with PD-L1 in the absence of small molecule) suggest that the phenotype was PD-L1 specific. But as we have shown above, the results from Aurigene's cell-based assays cannot be attributed to direct inhibition of PD-1/PD-L1 binding. Instead, it would appear that an alternative mechanism is responsible for the observed phenotypic effect.

Despite the recent appearance of a number of papers related to small molecule modulation of the PD-1/PDL-1 interaction,[14,28,31,41-44] there is little explanation of how the Aurigene compounds exert their function. However, a close reading of Aurigene's patent portfolio provides some insight into the development of this class of small molecules. Aurigene's early patent filings claimed large peptides that mimic a significant portion of the PD-1 extracellular domain (Figure 4A).[33] This includes much of the PD-L1 binding interface, and so it is likely that these large peptides would be competitive inhibitors of the PD-1/PD-L1 interaction. Attempts to achieve more drug-like properties, however, led to subsequent filings describing the development of macrocyclic peptides that mimic the 7-residue BC-loop (Figure 4B).[34] The most recent filings further refine the structure (and, presumably, improve the pharmacokinetic properties) by developing small tripeptides and peptidomimetic analogues that mimic the central serine-asparagine-threonine tripeptide of this loop (Figure 4C).[35–37] This is the strategy that ultimately led to small molecules **1**–**3**.

Critically, however, the BC-loop (and particularly the region mimicked by **1**–**3**) points away from the PD-L1 binding interface (Figure 4B) and so it is unclear why these molecules would be expected to be direct binding inhibitors, notwithstanding their apparent potency in cell-based assays and the fact that they are referred to (with little supporting data) in Aurigene's patents[35–37] and subsequent reviews[28,42,45] as inhibitors of the PD-1/PD-L1 interaction.

While it is possible that there is some key difference (e.g. glycosylation state) between our *in vitro* system and the 'real-life' PD-1 and PD-L1 proteins expressed on the surface of T cells and antigen presenting cells, a more likely scenario is that the compounds do mimic the PD-1 surface as intended, but that this serves not to directly disrupt binding with the PD-L1 protein as has been assumed, but perhaps to modulate the function of some other PD-1 binding partner. Both PD-1 and PD-L1 are thought to participate in regulatory binding interactions with other proteins,[46,47] and we hypothesize that one or more of these might be the true biological target of **1**–**3**.

In 2015, Curis Inc. initiated clinical trials with a small molecule called CA-170, that had been developed at Aurigene.[48] The exact structure of CA-170 has yet to be disclosed, but this lead candidate apparently emerged from a focused library at Aurigene that was designed to exploit hotspots within the PD-1/PD-L1 complex.[49] In a recent review by two of the inventors of the Aurigene molecules **1**–**3**, it is stated that CA-170 was designed to target one or more conserved pockets found in PD-L1 and VISTA, a non-redundant immunosuppressing protein of the B7-superfamily.[28] These authors are careful to not indicate whether CA-170 is structurally related to compounds **1**–**3**, but two subsequent reviews (from two different groups) both speculate that CA-170 is related to Aurigene's earlier disclosed compounds.[50,51] One of these recent reviews asserts that CA-170 is an oxadiazole (like compounds **2** and **3**),[51] while the other describes CA-170 as a molecule capable of disrupting the PD-1/PD-L1 complex.[50] The existence of a clinical candidate that is likely related to compounds **1**–**3**, and that is thought to function through direct blockade of PD-1/PD-L1 binding, provides motivation to better understand the function for this series of small molecules. In this study, we performed surface-plasmon resonance assays to test the hypothesis of direct protein binding inhibition and found that none of the compounds tested can disrupt the interaction between soluble PD-1 and adhered PD-L1 or between soluble PD-L1 and adhered PD-1. Preliminary testing also did not reveal binding of **1**–**3** to surface-bound VISTA (Figure S7). Based on these data and an analysis of structural features of the PD-1/PD-L1 interaction (and particularly the region of the PD-1 BC-loop from which Aurigene's lead compounds were derived) we hypothesize

that this family of small molecules may regulate the function of some other PD-1 binding partner.[52]

ASSOCIATED CONTENT

Supporting Information

The Supporting Information is available free of charge on the ACS Publications website.

Supplementary Figures S1–S8, together with experimental details for protein expression, analytical methods, and compound synthesis, as well as NMR spectra for synthesized compounds **1**–**4** (PDF)

AUTHOR INFORMATION

Corresponding Author

* E-mail: wulff@uvic.ca.

Author Contributions

The manuscript was written through contributions of all authors. All authors have given approval to the final version of the manuscript.

Funding Sources

This work was supported by funding from the Canadian Cancer Society Research Institute (grant # 701684), as well as an NSERC CREATE grant (# 497311-2017) and an NSERC Discovery grant to J.W. (# 4283). Additional support came from the Michael Smith Foundation for Health Research, the Canada Research Chairs program, and the University of Victoria.

Notes

D.A.P. is an employee of Inception Sciences Canada. The remaining authors declare no competing financial interest.

ACKNOWLEDGMENT

D.J.B. thanks the Polymer Nanoparticles for Drug Delivery (POND) CREATE program for a stipend and the University of Victoria for partial operating support that was used to offset the cost of this research. F.H. and J.W. thank the Canada Research Chairs program for salary support.

ABBREVIATIONS

PD-1, programed cell death protein 1 (CD279); PD-L1, programed death-ligand 1 (CD274 or B7-H1); VISTA, V-domain Ig suppressor of T cell activation; SPR, surface plasmon resonance.

REFERENCES

(1) Santarpia, M.; González-Cao, M.; Viteri, S.; Karachaliou, N.; Altavilla, G.; Rosell, R. Programmed Cell Death Protein-1/Programmed Cell Death Ligand-1 Pathway Inhibition and Predictive Biomarkers: Understanding Transforming Growth Factor-Beta Role. *Transl. Lung Cancer Res.* **2015**, *4* (6), 728–742.

(2) Bally, A. P. R.; Austin, J. W.; Boss, J. M. Genetic and Epigenetic Regulation of PD-1 Expression. *J. Immunol.* **2016**, *196* (6), 2431–2437.

(3) Liang, S. C.; Latchman, Y. E.; Buhlmann, J. E.; Tomczak, M. F.; Horwitz, B. H.; Freeman, G. J.; Sharpe, A. H. Regulation of PD-1, PD-L1, and PD-L2 Expression during Normal and Autoimmune Responses. *Eur. J. Immunol.* **2003**, *33* (10), 2706–2716.

(4) Shi, L.; Chen, S.; Yang, L.; Li, Y. The Role of PD-1 and PD-L1 in T-Cell Immune Suppression in Patients with Hematological Malignancies. *J. Hematol. Oncol.* **2013**, *6* (1), 74–79.

(5) Geng, L.; Huang, D.; Liu, J.; Qian, Y.; Deng, J.; Li, D.; Hu, Z.; Zhang, J.; Jiang, G.; Zheng, S. B7-H1 up-Regulated Expression in Human Pancreatic Carcinoma Tissue Associates with Tumor Progression. *J. Cancer Res. Clin. Oncol.* **2008**, *134* (9), 1021–1027.

(6) Soliman, H.; Khalil, F.; Antonia, S. PD-L1 Expression Is Increased in a Subset of Basal Type Breast Cancer Cells. *PLoS One* **2014**, *9* (2), e88557.

(7) Mu, C. Y.; Huang, J. A.; Chen, Y.; Chen, C.; Zhang, X. G. High Expression of PD-L1 in Lung Cancer May Contribute to Poor Prognosis and Tumor Cells Immune Escape through Suppressing Tumor Infiltrating Dendritic Cells Maturation. *Med. Oncol.* **2011**, *28* (3), 682–688.

(8) Azuma, K.; Ota, K.; Kawahara, A.; Hattori, S.; Iwama, E.; Harada, T.; Matsumoto, K.; Takayama, K.; Takamori, S.; Kage, M.; Hoshino, T.; Nakanishi, Y.; Okamoto, I. Association of PD-L1 Overexpression with Activating EGFR Mutations in Surgically Resected Nonsmall-Cell Lung Cancer. *Ann. Oncol.* **2014**, *25* (10), 1935–1940.

(9) Zhu, X.; Lang, J. Soluble PD-1 and PD-L1: Predictive and Prognostic Significance in Cancer. *Oncotarget* **2017**, *8* (57), 97671–97682.

(10) Saito, R.; Abe, H.; Kunita, A.; Yamashita, H.; Seto, Y.; Fukayama, M. Overexpression and Gene Amplification of PD-L1 in Cancer Cells and PD-L1 + Immune Cells in Epstein-Barr Virus-Associated Gastric Cancer: The Prognostic Implications. *Mod. Pathol.* **2017**, *30* (3), 427–439.

(11) Qin, T.; Zeng, Y.; Qin, G.; Xu, F.; Lu, J.; Fang, W.; Xue, C.; Zhan, J.; Zhang, X.; Zheng, Q.; Peng, R.; Yuan, Z.; Zhang, L.; Wang, S. High PD-L1 Expression Was Associated with Poor Prognosis in 870 Chinese Patients with Breast Cancer. *Oncotarget* **2015**, *6* (32), 33792–33981.

(12) Shin, S.-J.; Jeon, Y. K.; Cho, Y. M.; Lee, J.-L.; Chung, D. H.; Park, J. Y.; Go, H. The Association Between PD-L1 Expression and the Clinical Outcomes to Vascular Endothelial Growth Factor-Targeted Therapy in Patients With Metastatic Clear Cell Renal Cell Carcinoma. *Oncologist* **2015**, *20* (11), 1253–1260.

(13) Gong, J.; Chehrazi-Raffle, A.; Reddi, S.; Salgia, R. Development of PD-1 and PD-L1 Inhibitors as a Form of Cancer Immunotherapy: A Comprehensive Review of Registration Trials and Future Considerations. *J. Immunother. Cancer* **2018**, *6* (1), 8–25.

(14) Li, Y.; Li, F.; Jiang, F.; Lv, X.; Zhang, R.; Lu, A.; Zhang, G. A Mini-Review for Cancer Immunotherapy: Molecular Understanding of PD-1/ PD-L1 Pathway & Translational Blockade of Immune Checkpoints. *Int. J. Mol. Sci.* **2016**, *17* (7), 1151–1172.

(15) Alsaab, H. O.; Sau, S.; Alzhrani, R.; Tatiparti, K.; Bhise, K.; Kashaw, S. K.; Iyer, A. K. PD-1 and PD-L1 Checkpoint Signaling Inhibition for Cancer Immunotherapy: Mechanism, Combinations, and Clinical Outcome. *Front. Pharmacol.* **2017**, *8* (561), 1–20.

(16) Zhan, M. M.; Hu, X. Q.; Liu, X. X.; Ruan, B. F.; Xu, J.; Liao, C. From Monoclonal Antibodies to Small Molecules: The Development of Inhibitors Targeting the PD-1/PD-L1 Pathway. *Drug Discov. Today* **2016**, *21* (6), 1027–1036.

(17) Markham, A.; Duggan, S. Cemiplimab: First Global Approval. *Drugs* **2018**, *78* (17), 1841–1846.

(18) Wojas-Krawczyk, K.; Kalinka, E.; Grenda, A.; Krawczyk, P.; Milanowski, J. Beyond PD-L1 Markers for Lung Cancer Immunotherapy. *Int. J. Mol. Sci.* **2019**, *20* (8), 1915–1932.

(19) Borghaei, H.; Paz-Ares, L.; Horn, L.; Spigel, D. R.; Steins, M.; Ready, N. E.; Chow, L. Q.; Vokes, E. E.; Felip, E.; Holgado, E.; et al. Nivolumab versus Docetaxel in Advanced Nonsquamous Non-Small-Cell Lung Cancer. *N. Engl. J. Med.* **2015**, *373* (17), 1627–1639.

(20) Brahmer, J.; Reckamp, K. L.; Baas, P.; Crinò, L.; Eberhardt, W. E. E.; Poddubskaya, E.; Antonia, S.; Pluzanski, A.; Vokes, E. E.; Holgado, E.; et al. Nivolumab versus Docetaxel in Advanced Squamous-Cell Non-Small-Cell Lung Cancer. *N. Engl. J. Med.* **2015**, *373* (2), 123–135.

(21) Herbst, R. S.; Baas, P.; Kim, D. W.; Felip, E.; Pérez-Gracia, J. L.; Han, J. Y.; Molina, J.; Kim, J. H.; Arvis, C. D.; Ahn, M. J.; et al. Pembrolizumab versus Docetaxel for Previously Treated, PD-L1-Positive, Advanced Non-Small-Cell Lung Cancer (KEYNOTE-010): A Randomised Controlled Trial. *Lancet* **2016**, *387* (10027), 1540–1550.

(22) Reck, M.; Rodríguez-Abreu, D.; Robinson, A. G.; Hui, R.; Csőszi, T.;

Fülöp, A.; Gottfried, M.; Peled, N.; Tafreshi, A.; Cuffe, S.; et al. Pembrolizumab versus Chemotherapy for PD-L1–Positive Non–Small-Cell Lung Cancer. *N. Engl. J. Med.* **2016**, *375* (19), 1823–1833.

(23) Rittmeyer, A.; Barlesi, F.; Waterkamp, D.; Park, K.; Ciardiello, F.; von Pawel, J.; Gadgeel, S. M.; Hida, T.; Kowalski, D. M.; Dols, M. C.; et al. Atezolizumab versus Docetaxel in Patients with Previously Treated Non-Small-Cell Lung Cancer (OAK): A Phase 3, Open-Label, Multicentre Randomised Controlled Trial. *Lancet* **2017**, *389* (10066), 255–265.

(24) Apolo, A. B.; Infante, J. R.; Balmanoukian, A.; Patel, M. R.; Wang, D.; Kelly, K.; Mega, A. E.; Britten, C. D.; Ravaud, A.; Mita, A. C.; Safran, H.; Stinchcombe, T. E.; Srdanov, M.; Gelb, A. B.; Schlichting, M.; Chin, K.; Gulley, J. L. Avelumab, an Anti–Programmed Death-Ligand 1 Antibody, In Patients With Refractory Metastatic Urothelial Carcinoma: Results From a Multicenter, Phase Ib Study. *J. Clin. Oncol.* **2017**, *35* (19), 2117–2124.

(25) Antonia, S. J.; Villegas, A.; Daniel, D.; Vicente, D.; Murakami, S.; Hui, R.; Yokoi, T.; Chiappori, A.; Lee, K. H.; de Wit, M.; et al. Durvalumab after Chemoradiotherapy in Stage III Non–Small-Cell Lung Cancer. *N. Engl. J. Med.* **2017**, *377* (20), 1919–1929.

(26) Chames, P.; Van Regenmortel, M.; Weiss, E.; Baty, D. Therapeutic Antibodies: Successes, Limitations and Hopes for the Future. *Br. J. Pharmacol.* **2009**, *157* (2), 220–233.

(27) Liu, J. K. H. The History of Monoclonal Antibody Development - Progress, Remaining Challenges and Future Innovations. *Ann. Med. Surg.* **2014**, *3* (4), 113–116.

(28) Sasikumar, P. G.; Ramachandra, M. Small-Molecule Immune Checkpoint Inhibitors Targeting PD-1/PD-L1 and Other Emerging Checkpoint Pathways. *BioDrugs* **2018**, *32* (5), 481–497.

(29) Chupak, L.; Zheng, X. Compounds as Useful Immunomodulators. WO2015034820A1, 2014.

(30) Sharpe, A. H.; Butte, M. J.; Oyama, S. Modulators of Immunoinhibitory Receptor Pd-1, and Methods of Use Thereof. WO2011082400A2, 2011.

(31) Li, K.; Tian, H. Development of Small-Molecule Immune Checkpoint Inhibitors of PD-1/PD-L1 as a New Therapeutic Strategy for Tumour Immunotherapy. *J. Drug Target.* **2018**, *1*, 1–13.

(32) Konstantinidou, M.; Zarganes-Tzitzikas, T.; Magiera-Mularz, K.; Holak, T. A.; Dömling, A. Immune Checkpoint PD-1/PD-L1: Is There Life Beyond Antibodies? *Angew. Chemie - Int. Ed.* **2018**, *57* (18), 4840–4848.

(33) Sasikumar, P. G. N.; Ramachandra, M.; Vadlamani, S. K.; Vemula, K. R.; Satyam, L. K.; Subbarao, K.; Shrimali, K. R.; Kandepu, S. Immunosuppression Modulating Compounds. US2011031873A1, 2011.

(34) Sasikumar, P. G. N.; Ramachandra, M. Immunomodulating Cyclic Compounds from the Bc Loop of Human Pd1. WO2013144704A1, 2013.

(35) Sasikumar, P. G. N.; Ramachandra, M.; Naremaddepalli, S. S. S. Peptidomimetic Compounds as Immunomodulators. US20130237580, 2013.

(36) Sasikumar, P. G. N.; Ramachandra, M.; Naremaddepalli, S. S. S. 1,2,4-Oxadiazole Derivatives As Immunomodulators. WO2015033299A1, 2014.

(37) Sasikumar, P. G. N.; Ramachandra, M.; Prasad, A.; Naremaddepalli, S. S. S. 3-Substituted-1,2,4-Oxadiazole and Thiadiazole Compounds As Immunomodulators. WO2016142886A2, 2016.

(38) Zak, K. M.; Grudnik, P.; Guzik, K.; Zieba, B. J.; Musielak, B.; Dömling, A.; Dubin, G.; Holak, T. A.; Zak, K. M.; Grudnik, P.; Guzik, K.; Zieba, B. J.; Musielak, B.; Dömling, A.; Dubin, G.; Holak, T. A. Structural Basis for Small Molecule Targeting of the Programmed Death Ligand 1 (PD-L1). *Oncotarget* **2016**, *7* (21), 30323–30335.

(39) Hanley, R. Inhibitors of the PD1/PD-L1 Interaction: Missteps, Mechanisms, and Mysteries, Unversity of Victoria, 2017.

(40) Skalniak, L.; Zak, K. M.; Guzik, K.; Magiera, K.; Musielak, B.; Pachota, M.; Szelazek, B.; Kocik, J.; Grudnik, P.; Tomala, M.; Krzanik, S.; Pyrc, K.; Dömling, A.; Dubin, G.; Holak, T. A. Small-Molecule Inhibitors of PD-1/PD-L1 Immune Checkpoint Alleviate the PD-L1-Induced Exhaustion of T-Cells. *Oncotarget* **2017**, *8* (42), 72167–72181.

(41) Weinmann, H. Cancer Immunotherapy: Selected Targets and Small-Molecule Modulators. *ChemMedChem* **2016**, *11* (5), 450–466.

(42) Zarganes-Tzitzikas, T.; Konstantinidou, M.; Gao, Y.; Krzemien, D.; Zak, K.; Dubin, G.; Holak, T. A.; Dömling, A. Inhibitors of Programmed Cell Death 1 (PD-1): A Patent Review (2010-2015). *Expert Opin. Ther. Pat.* **2016**, *26* (9), 973–977.

(43) Magiera-Mularz, K.; Skalniak, L.; Zak, K. M.; Musielak, B.; Rudzinska-Szostak, E.; Berlicki, Ł.; Kocik, J.; Grudnik, P.; Sala, D.; Zarganes-Tzitzikas, T.; Shaabani, S.; Dömling, A.; Dubin, G.; Holak, T. A. Bioactive Macrocyclic Inhibitors of the PD-1/PD-L1 Immune Checkpoint. *Angew. Chemie Int. Ed.* **2017**, *56* (44), 13732–13735.

(44) Hanley, R. P.; Horvath, S.; An, J.; Hof, F.; Wulff, J. E. Salicylates Are Interference Compounds in TR-FRET Assays. *Bioorganic Med. Chem. Lett.* **2016**, *26* (3), 973–977.

(45) Chen, T.; Li, Q.; Liu, Z.; Chen, Y.; Feng, F.; Sun, H. Peptide-Based and Small Synthetic Molecule Inhibitors on PD-1/PD-L1 Pathway: A New Choice for Immunotherapy? *Eur. J. Med. Chem.* **2019**, *161*, 378–398.

(46) Sharpe, A. H.; Pauken, K. E. The Diverse Functions of the PD1 Inhibitory Pathway. *Nature Reviews Immunology*. Nature Publishing Group November 13, 2018, pp 153–167.

(47) Butte, M. J.; Peña-Cruz, V.; Kim, M.-J.; Freeman, G. J.; Sharpe, A. H. Interaction of Human PD-L1 and B7-1. *Mol. Immunol.* **2008**, *45* (13), 3567–3572.

(48) Curis Inc. A Study of CA-170 (Oral PD-L1, PD-L2 and VISTA Checkpoint Antagonist) in Patients With Advanced Tumors and Lymphomas - Full Text View - ClinicalTrials.gov https://clinicaltrials.gov/ct2/show/NCT02812875 (accessed Mar 25, 2019).

(49) Yang, J.; Hu, L. Immunomodulators Targeting the PD-1/PD-L1 Protein-Protein Interaction: From Antibodies to Small Molecules. *Med. Res. Rev.* **2019**, *39* (1), 265–301.

(50) Huck, B. R.; Kötzner, L.; Urbahns, K. Small Molecules Drive Big Improvements in Immuno-Oncology Therapies. *Angew. Chemie* **2018**, *57*, 412–4428.

(51) Wang, T.; Wu, X.; Guo, C.; Zhang, K.; Xu, J.; Li, Z.; Jiang, S. Development of Inhibitors of the Programmed Cell Death-1/Programmed Cell Death-Ligand 1 Signaling Pathway. *Journal of Medicinal Chemistry*. American Chemical Society February 28, 2019, pp 1715–1730.

(52) Following the submission of this manuscript, a study on the *in vitro* function of a likely CA-170 candidate (structurally related to **1**–**3**) was disclosed. This study likewise finds that the candidate is inactive in a variety of protein-binding experiments, and concludes that an alternative mechanism may be responsible for its biological activity. See: Musielak, B.; Kocik, J.; Skalniak, L.; Magiera-Mularz, K.; Sala, D.; Czub, M.; Holak, T. A.; Plewka, J. CA-170 - a Potent Small-Molecule PD-L1 Inhibitor or Not? bioRxiv 662668; doi: https://doi.org/10.1101/662668.

TOC graphic (1.75” x 3”, at 600 dpi):

In Vitro Assessment of Putative PD-1/PD-L1 Inhibitors: Suggestions of an Alternative Mode of Action.

Derek J. Blevins,† Ronan Hanley,† Trevor Bolduc,† David A. Powell,‡ Michael Gignac,† Kayleigh Walker,§ Mark D. Carr,§ Fraser Hof,† and Jeremy E. Wulff *,†

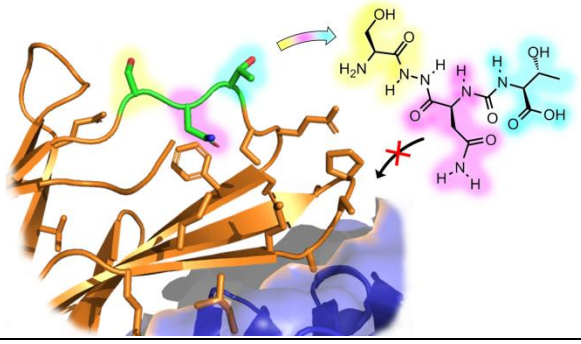

Supporting Information for:

In Vitro Assessment of Putative PD-1/PD-L1 Inhibitors: Suggestions of an Alternative Mode of Action

Derek J. Blevins, Ronan Hanley, Trevor Bolduc, David A. Powell, Michael Gignac, Kayleigh Walker, Mark D. Carr, Fraser Hof, and Jeremy E. Wulff

Index

Supplementary Figures

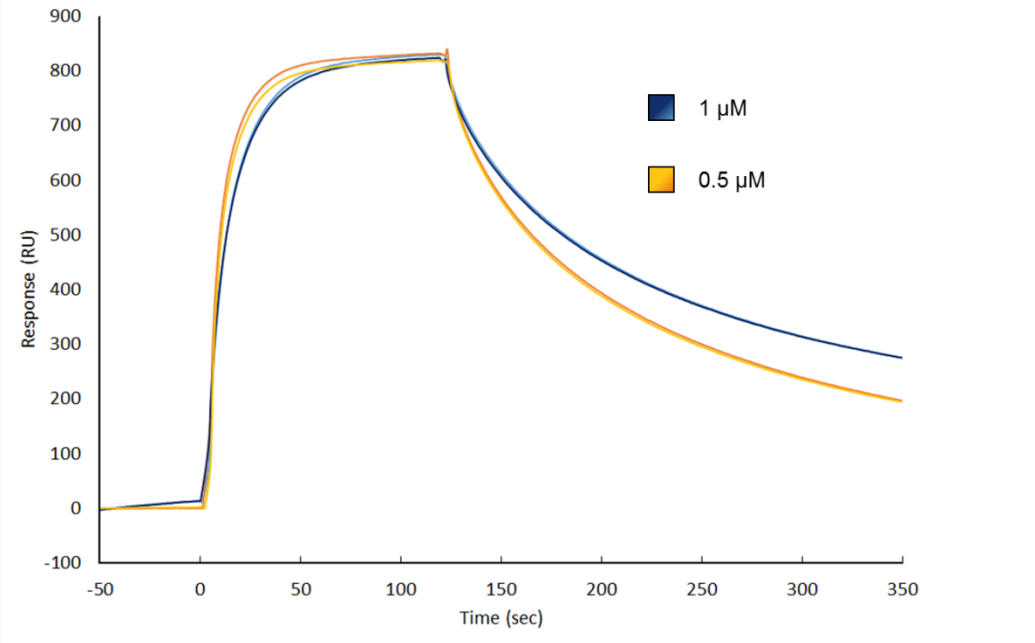

Figure S1. Representative sensorgrams for PD-1 binding to surface-bound PD-L1. The legend indicates the concentration of PD-1 used in each duplicate experiment.

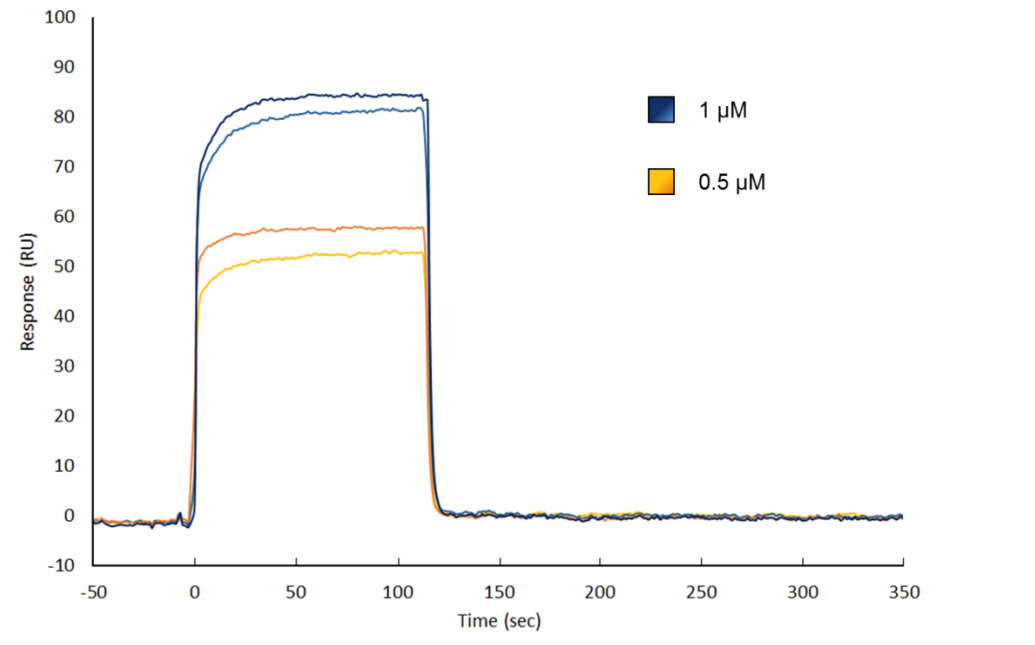

Figure S2. Representative sensorgrams for PD-L1 binding to surface-bound PD-1. The legend indicates the concentration of PD-L1 used in each duplicate experiment.

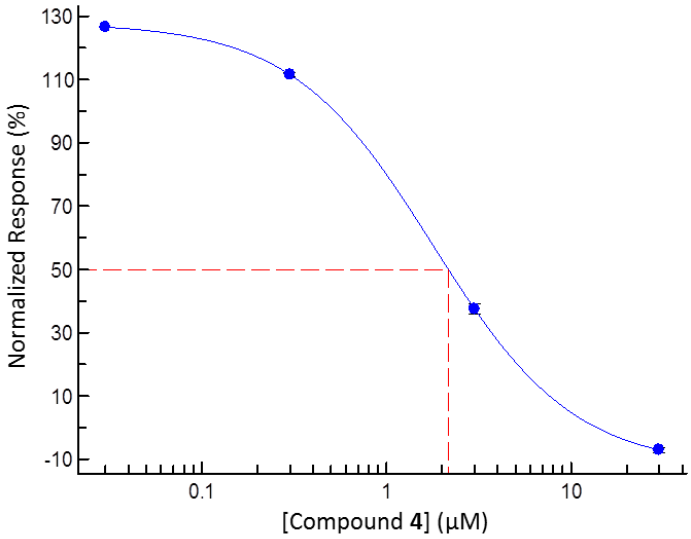

Figure S3. Titration of compound **4** as an inhibitor of soluble PD-1 (at 15 µM) binding to a PD-L1 SA chip. The measured IC_{50} was 2.2 µM. This is a much higher than the typical nanomolar potency reported for compound **4** (see references 29 and 38–40, as well as the data in Figure 2, Figure 3, and Figure S8), due to the extremely high protein concentrations necessary to observe saturation of binding within the experiment.

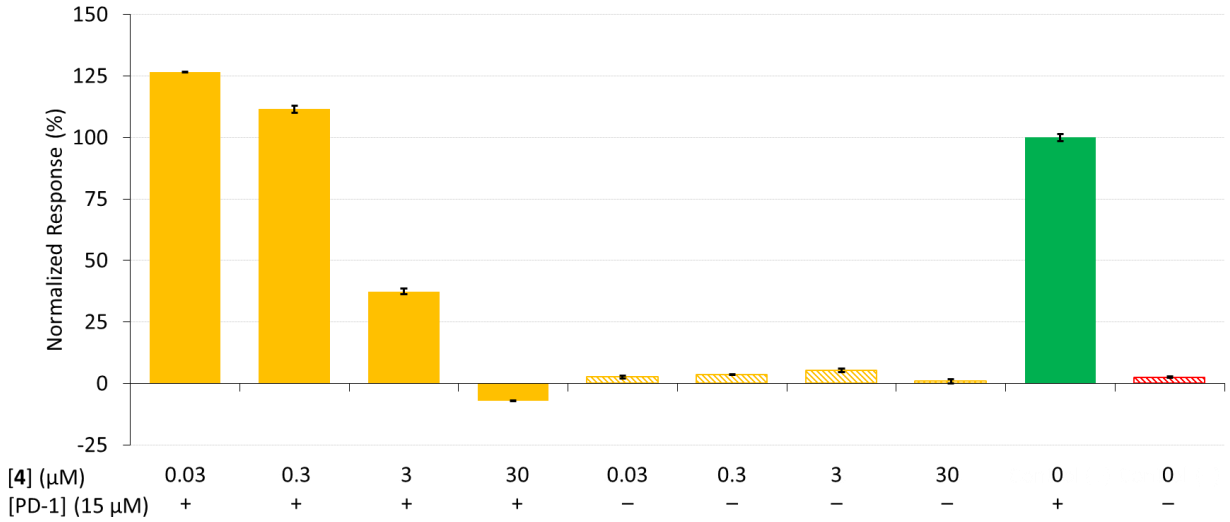

Figure S4. Complete SPR data (including measurements with and without soluble PD-1) demonstrating inhibition of the PD-1/PD-L1 interaction with compound **4**. Soluble PD-1 (at 15 µM) was flowed across surface-bound PD-L1 with and without compound **4** at varying concentrations. The response is normalized to the control protein interaction (PD-1 only). Error bars represent variance between duplicate analyses. Hashed bars indicate control experiments performed with no PD-1 protein.

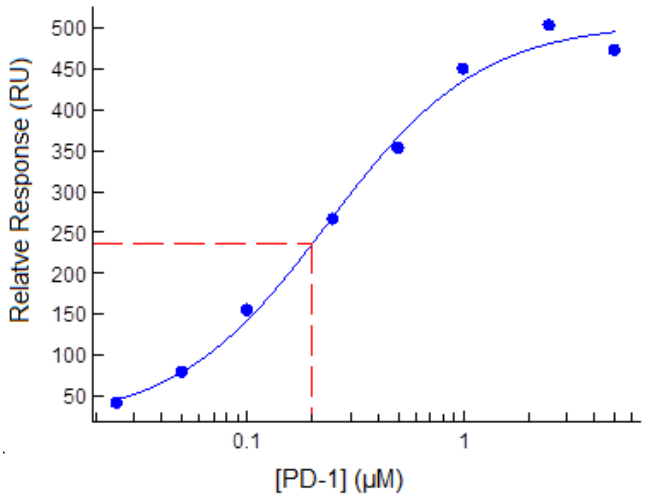

Figure S5. Measurement of the affinity for soluble PD-1 to surface-bound PD-L2. The effective K_D for the interaction was determined to be 199 nM by SPR.

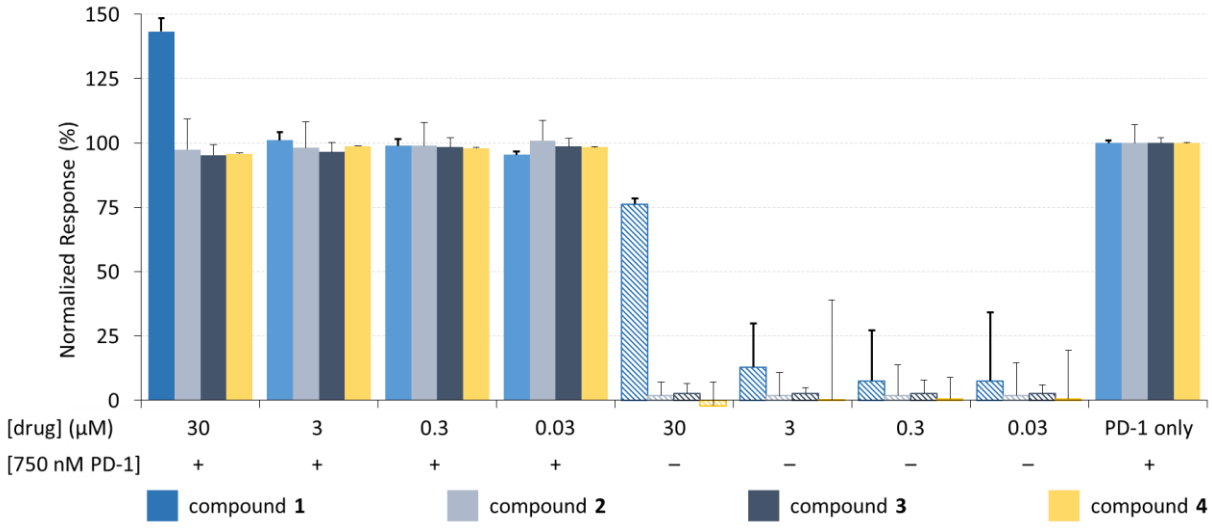

Figure S6. Neither the Aurigene compounds (**1**–**3**) nor the BMS compound (**4**) were effective inhibitors of the PD-1/PD-L2 interaction, nor do any of the tested compound bind directly to surface-bound PD-L2. Soluble PD-1 was flowed across surface-bound PD-L2 with and without test compounds at various concentrations. The response is normalized to the control protein concentration (PD-1 only). Responses were measured in triplicate and error bars represent standard deviation. Hashed bars indicate control experiments performed with no PD-1 protein.

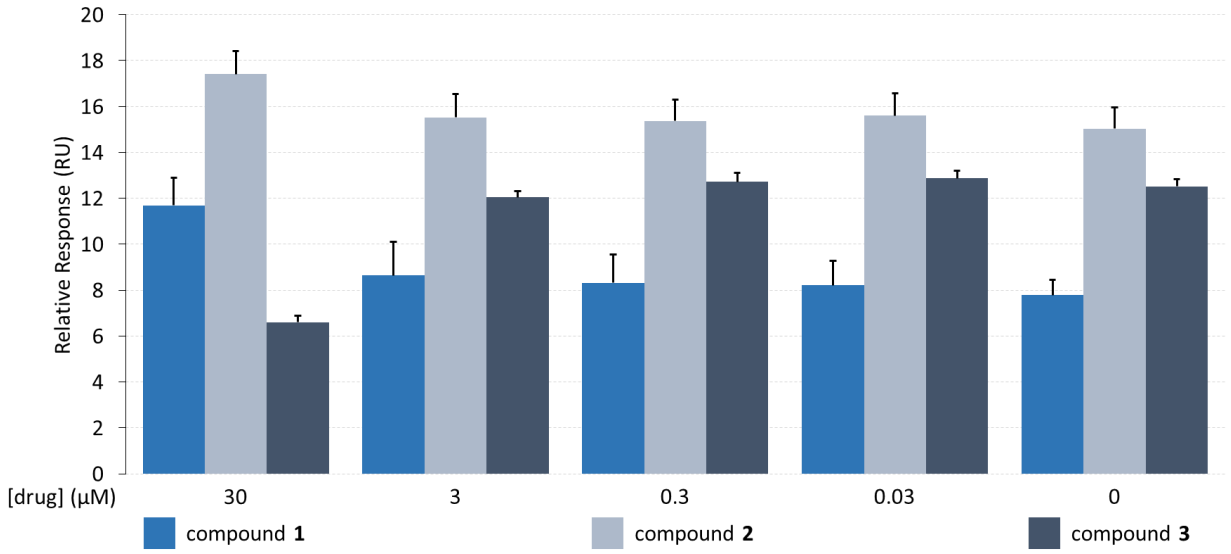

Figure S7. The Aurigene compounds (**1**–**3**) do not bind to surface-bound VISTA protein. Test compounds at four different concentrations were flowed across surface-bound VISTA, but no significant binding (relative to the blank sample) was detected. Responses were measured in triplicate and error bars represent standard deviation. The expected maximal responses were 44, 25, and 42 RU for binding of any of the compounds **1**–**3**, respectively.

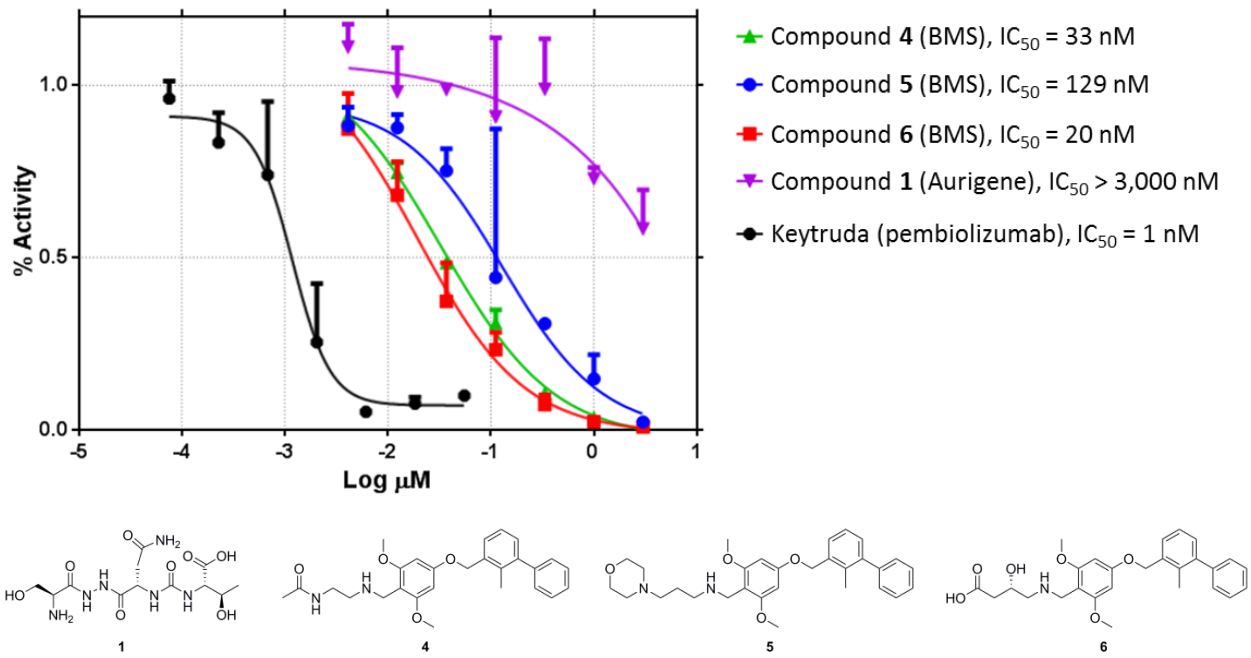

Figure S8. In a confirmatory ELISA assay, three compounds claimed by BMS (**4**–**6**) showed potent inhibition of the PD-1/PD-L1 interaction, but the Aurigene compound **1** showed no significant inhibition.

Materials and Methods

1. Expression, Refolding, and Purification of Extracellular PD-L1

E. coli BL21(DE3) cells were transfected with a pET28a(+) vector containing the sequence for the extracellular region of PD-L1 (A18-T239) with codon usage optimized for expression in *E. coli*. Cells were cultured in LB media treated with 50 µg/mL Kanamycin at 37 ^{o}C to an OD_{600} of 0.9. PD-L1 expression as insoluble inclusion bodies was then induced with the addition of 1 mM IPTG. The cells were cultured for a further 5 hours before being collected by centrifugation. Cell pellets from 1 L culture were resuspended in 35 mL phosphate-based saline (137 mM NaCl, 2.7 mM KCl, 10 mM Na_2HPO_4, 1.8 mM KH_2PO_4, pH 7.4) treated with protease inhibitors (Roche), and lysed by sonication. Inclusion bodies containing PD-L1 were collected from the cell lysate by centrifugation at 15,000 RPM for 20 minutes. Inclusion body pellets were then washed three times by resuspension in wash buffer followed by centrifugation. The first two washes were performed using a buffer containing 50 mM Tris, pH 8.0, 200 mM NaCl, 10 mM EDTA, 0.5% (v/v) Triton-X100, 10 mM DTT. The final wash was done in the same buffer excluding the detergent. Washed inclusion body pellets from 1 L original culture were resolubilized by shaking for 1 hour at 37^{o}C in 20 mL resolubilization buffer (50 mM Tris buffer, pH 8.0, 5 M guanidine, 200 mM NaCl, 20 mM DTT). Resolubilized PD-L1 was refolded by drop-wise dilution 100-fold into refolding buffer (100 mM Tris, pH 8.0, 1 M arginine, 0.5 mM glutathione$_{ox}$, 2 mM glutathione$_{red}$). The refolding mixture was then concentrated by tangential flow filtration before being dialyzed into gel filtration buffer (10 mM Tris, pH 8.0, 20 mM NaCl). Folded PD-L1 was separated from misfolded aggregates and contaminants by size exclusion chromatography using a 16/60 Superdex 75 column (GE Healthcare) equilibrated with 10 mM Tris, pH 8.0, 20 mM NaCl. The purified protein was verified by SDS-PAGE as a band at 25 kDa.

2. Expression, Refolding, and Purification of Extracellular PD-1

E. coli BL21-CodonPlus RIL was transfected with a pET28a(+) vector containing the sequence for the extracellular domain of PD-1 (P34-E150). The strain was grown in LB media treated with 50 µg/mL Kanamycin overnight at 37 °C to an OD_{600} of 0.9. 1 mM. IPTG was added to induce expression of the vector, and the culture was incubated another 4 hours after induction. The cultures were then spun down at 4 °C. The pellets were resuspended in 35 mL phosphate-based saline (137 mM NaCl, 2.7 mM KCl, 10 mM Na_2HPO_4, 1.8 mM KH_2PO_4, pH 7.4) treated with protease inhibitors (Millipore), and lysed by sonication. The cell lysate was spun down twice at 15,000 RPM for 20 minutes to pellet inclusion bodies of protein. The inclusion bodies were resuspended by a glass homogenizer in 30 mL wash buffer (100 mM Tris, pH 8.0, 200 mM NaCl, 10 mM EDTA, 0.5% (v/v) Triton-X100, 10 mM DTT). This was performed a second time with the absence of Triton-X100. The inclusion bodies were then resolubilized in 20 mL suspension buffer (100 mM Tris buffer, pH 8.0, 5 M guanidine, 200 mM NaCl, 20 mM DTT) and left to shake for 1 hour at 37 °C. This suspension was centrifuged for 20 minutes at 15000 rpm. The solution was resolubilized and added dropwise dilute 100-fold in stirred refold buffer (100 mM Tris buffer, pH 8.0, 0.4 M arginine, 2 mM EDTA, 0.5 mM glutathione$_{ox}$, 2 mM glutathione$_{red}$) at 4 °C and let stir overnight. The resulting solution containing PD-1 protein was then concentrated to 50 mL and dialyzed into gel filtration buffer (10 mM Tris buffer, pH 8.0, 20 mM NaCl) for purification. Protein was purified by

size exclusion chromatography at 78 mL by Superdex S75 exclusion column. The purified protein was verified by SDS-PAGE as a band at 13 kDa. The concentrated protein was then dialyzed in appropriate HBS-EP+ running buffer for SPR analyses.

3. SPR Binding Assays

All SPR related materials and buffer were manufactured by GE Healthcare Lifesciences unless otherwise noted. Assays were performed on a BiaCore X100 with no changes to sample flow and binding parameters.

All chips were immobilized with their respective protein under the default conditions for an aimed response level. The target immobilized response was calculated to give an expected R_{max} of 100 RU based on the equation 1, where the MW is the molecular weight of the ligand (immobilized protein) or the analyte (compounds being flowed). The immobilization was run under default conditions provided by the BiaCore X100 (GE Healthcare Life Sciences).

$$R_{ligand} = \frac{R_{max} * MW_{ligand}}{MW_{analyte}} \quad \textbf{(1)}$$

3a. In vitro binding assay: Adsorbed Human PD-1

Human biotinylated-PD-1 (BPS Bioscience, Catalog 71106) was adsorbed to a gold surface by binding to streptavidin-coated sensor chip (SA chip, GE Healthcare). The ligand response (R_{ligand}) was 2029.9 RU. The analytes were flowed through with HBS-EP$^+$ (10 mM HEPES buffer, pH 7.4, 150 mM NaCl, 3 mM EDTA, 0.05% (v/v) P20, 0.5% (w/v) DMSO) at a concentration of 100 nM at 10 µL/min. Each of the compounds, **1**–**4**, were titrated by SPR to determine their ability to inhibit the PD-1/PD-L1 interaction. The concentration of PD-L1 was held constant at 500 nM. Compound **1**–**4** were also titrated in the absence of PD-L1, to determine their ability to bind to the adsorbed PD-1.

3b. In vitro binding assay: Adsorbed Human PD-L1

Human biotinylated-PD-L1 (BPS Bioscience, Catalog 71105) was adsorbed to a gold surface by binding to a separate SA chip (GE Healthcare). PD-L1 was immobilized from 100 nM aliquot with a final ligand response (R_{ligand}) of 2681.8 RU. Compounds **1**–**4** were flowed across the chip of adsorbed PD-L1 in the presence of PD-1 (1 µM) to determine their efficacy as inhibitors in triplicate, unless otherwise stated. Compound **1**–**4** were also titrated in the absence of PD-1, to determine their ability to bind to the adsorbed PD-L1.

3c. In vitro binding assay: Adsorbed Human PD-L2

Human biotinylated-PD-L2 (BPS Bioscience, Catalog 71108) was adsorbed to a gold surface by binding to another SA chip (GE Healthcare). The final response of the immobilized ligand was 3794.0 RU. Compounds **1**–**4** were titrated by flowing across the chip of adsorbed PD-L2 in the presence of PD-1 (0.75 µM) to determine their efficacy as inhibitors HBS-EP$^+$ buffer in triplicate. Compound **1**–**4** were also titrated in the absence of PD-1, to determine their ability to bind to the adsorbed PD-L2.

3d. In vitro binding assay: Adsorbed Human VISTA

Human biotinylated-VISTA (BPS Bioscience, Catalog 71327) was adsorbed to an SA chip (GE Healthcare) under continuous flow of HBS-EP$^+$. The final response of the immobilized ligand was 5482.6 RU. Compounds **1**–**4** were flowed across the chip of adsorbed VISTA to detect any potential binding in HBS-EP$^+$ buffer in triplicate.

4. Synthesis of Test Compounds

Compound **1** was synthesized by WuXi Apptec, following the protocol established in the patent from Aurigene, with minor modifications. Compounds **2** and **3** were synthesized by Santai Labs, following the protocol established in the patents from Aurigene. Compound **4** was synthesized in house, following the general protocol established in the patent from Bristol-Myers Squibb, with minor modifications. All final products were characterized by NMR and LCMS prior to use. Test solutions were assayed again by LCMS at the conclusion to the research, to confirm that they had not degraded during the time required to complete the measurements.

4a. Synthesis of Compound **1**

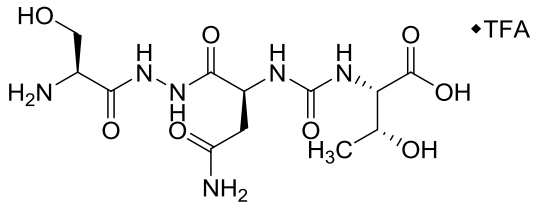

Compound **1**

This compound was described in US 2013/237580, Example 2 and similar chemistry was used herein to prepare this material at WuXi Apptec Co, Ltd. The characterization data for the compound is shown below. Nuclear Magnetic Resonance (NMR) analysis was conducted using a Varian 400 MHz spectrometer with an appropriate deuterated solvent. LCMS analysis was conducted using an Agilent 1200 & 1956A Waters Atlantis HILIC Silica 5 µM, 2.1 × 50 mm column, eluting with 90:10 to 40:60 H_2O:MeCN + 0.03% trifluoroacetic acid over 4 minutes at a flow rate of 0.6 mL/min. Detection methods are diode array (DAD) and evaporative light scattering (ELSD) detection as well as positive electrospray ionization. MS range was 100-1000.

Preparation of Intermediate A: Benzyl *O*-(*tert*-butyl)-*N*-(1*H*-imidazole-1-carbonyl)-*L*-threoninate

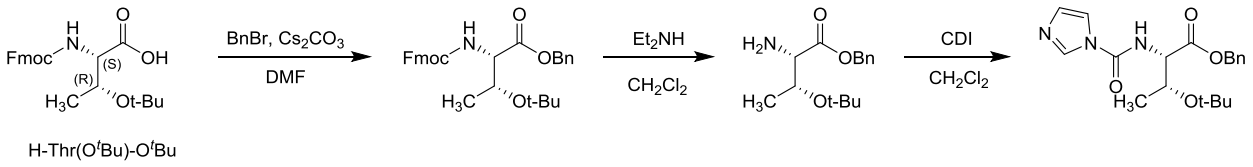

H-Thr(O^{t}Bu)-O^{t}Bu

Step 1: Synthesis of benzyl *N*-(((9*H*-fluoren-9-yl)methoxy)carbonyl)-*O*-(*tert*-butyl)-L-threoninate

To a solution of compound *N*-(((9*H*-fluoren-9-yl)methoxy)carbonyl)-*O*-(*tert*-butyl)-L-threonine (20.0 g, 50.3 mmol, 1.0 equiv, Fisher, CAS# 71989-35-0) in *N,N*-dimethylformamide (200 mL, 0.25 M) was added cesium carbonate (19.6 g, 60.4 mmol, 1.2 equiv) at 15 °C, the mixture was cooled to 0 °C and benzyl bromide (10.3 g, 60.4 mmol, 1.2 equiv) was added drop-wise. After stirring for 10 min, the mixture was warmed up to 15 °C and stirred for 16 h. TLC (petroleum ether/ethyl acetate = 2:1, Rf (SM) = 0.07, Rf (Prod) = 0.7) showed the starting material was consumed completely. The mixture was cooled to 5 °C and diluted with water (500 mL) and ethyl acetate (300 mL). The aqueous layer was extracted with ethyl acetate (2 × 200 mL) and the combined organic layers were washed with brine (200 mL), dried over anhydrous sodium sulfate and concentrated in vacuum. The residue was purified by silica gel chromatography (petroleum ether/ethyl acetate = 30:1-10:1) to give the title compound (22.8 g, 93% yield) as a white solid.

^{1}H NMR (400 MHz, $CDCl_3$) δ 7.70-7.68 (m, 2H), 7.65-7.50 (m, 2H), 7.32-7.23 (m, 9H), 5.55 (d, *J* = 9.0 Hz, 1H), 5.14 (d, *J* = 12.0 Hz, 1H), 5.01 (d, *J* = 12.0 Hz, 1H), 4.34-4.16 (m, 5H), 1.15 (d, *J* = 5.5 Hz, 3H), 1.03 (s, 9H).

Step 2: Synthesis of benzyl *O*-(*tert*-butyl)-*L*-threoninate

To a solution of benzyl *N*-(((9*H*-fluoren-9-yl)methoxy)carbonyl)-*O*-(*tert*-butyl)-L-threoninate (10.0 g, 20.5 mmol, 1.0 equiv) in anhydrous dichloromethane (100 mL, 0.2 M) was added *N,N*-diethylamine (7.5 g, 103 mmol, 5.0 equiv) at 15 °C, then the mixture was stirred at 15 °C for 12 h. TLC analysis (petroleum ether / ethyl acetate = 5:1, R_f (starting material = 0.4, product = 0)) showed the reaction was complete. The reaction mixture was concentrated under reduced pressure to give a residue. The residue was purified by column chromatography on silica gel (petroleum ether/ethyl acetate = 10:1) to give the title compound (4.5 g, 83% yield) as a yellow oil.

^{1}H NMR (400 MHz, $CDCl_3$) δ 7.37-7.26 (m, 5H), 5.20 (d, *J* = 12.0 Hz, 1H), 5.05 (d, *J* = 12.0 Hz, 1H), 4.04-3.99 (m, 1H), 3.32-3.31 (m, 1H), 1.23 (d, *J* = 6.0 Hz, 3H), 1.11 (s, 9H).

LRMS (LCMS, ESI+) calcd. for $C_{15}H_{24}NO_3$ $[M+H]^+$: 266, found 266.

Step 3: Synthesis of benzyl *N*-(((9*H*-fluoren-9-yl)methoxy)carbonyl)-*O*-(*tert*-butyl)-L-threoninate

To a solution of benzyl *O*-(*tert*-butyl)-*L*-threoninate (4.5 g, 16.9 mmol, 1.0 equiv) in anhydrous dichloromethane (50 mL, 0.34 M) was added a solution of di(imidazol-1-yl)methanone (4.12 g, 25.4 mmol, 1.5 equiv) in anhydrous dichloromethane (20 mL) at -20 °C, then the mixture was stirred at 0 °C for 2 h. LCMS showed the reaction was complete. The reaction was quenched with water (50 mL) and

the mixture was separated using a separatory funnel and the aqueous phase was extracted with dichloromethane (2 × 50 mL). The combined organic phases were washed with brine (50 mL), dried over anhydrous sodium sulfate and concentrated under reduced pressure to give afford the title compound (6.80 g, unpurified) as a colorless oil which was used directly in the next step.

LRMS (LCMS, ESI+) calcd. for $C_{19}H_{26}N_3O_4$ $[M+H]^+$: 360, found 360.

Preparation of (((*S*)-1-(2-(*L*-seryl)hydrazinyl)-4-amino-1,4-dioxobutan-2-yl)carbamoyl)-*L*-threonine trifluoracetate

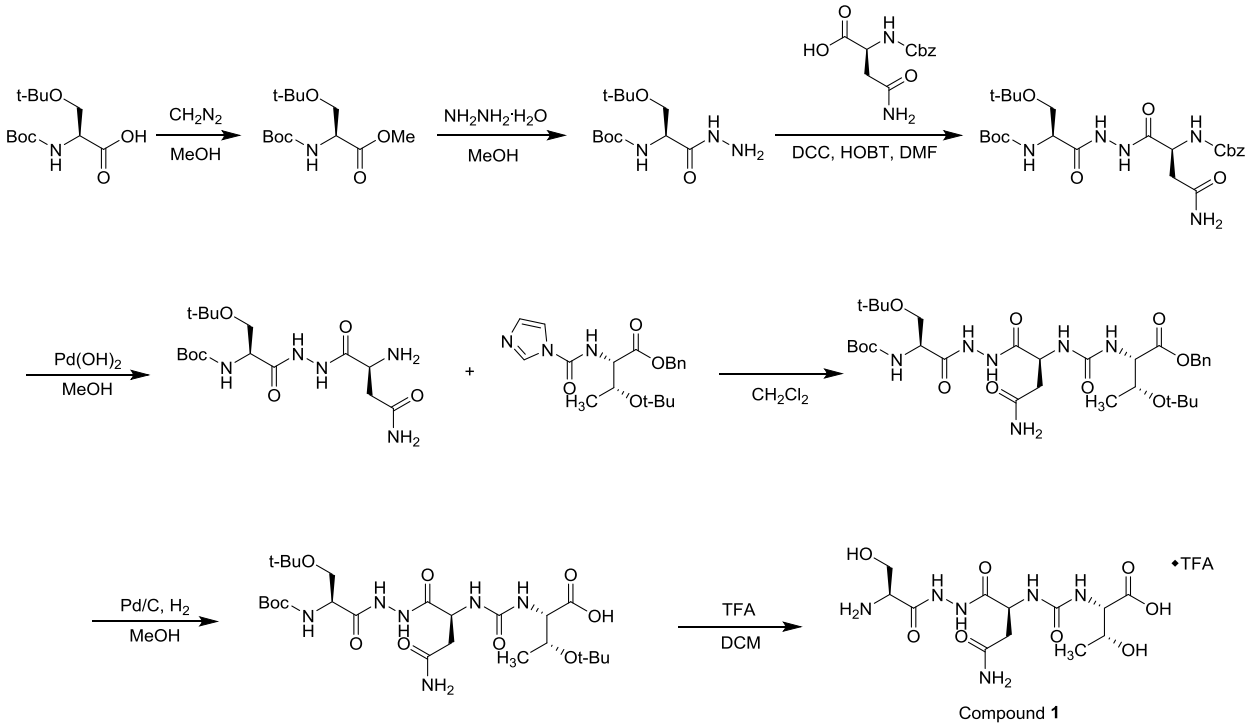

Step 1: Synthesis of methyl *N*-(*tert*-butoxycarbonyl)-*O*-(*tert*-butyl)-*L*-serinate

A solution of diazomethane (0.77 M, 397 mL, 4.0 equiv) in ether was decanted portion-wise to a solution of *N*-(*tert*-butoxycarbonyl)-*O*-(*tert*-butyl)-*L*-serine (20 g, 76.5 mmol, 1.0 equiv, Alfa Aesar CAS# 13734-38-8) in methanol (200 mL, 0.1 M) at -5 °C. After addition, the mixture was warmed to 15 °C and stirred for 16 h at this temperature. TLC analysis (methanol/dichloromethane = 10:1, Rf (SM) = 0.3, petroleum ether/ethyl acetate = 2:1, Rf (Prod) = 0.7) showed the starting material was consumed completely. The mixture was concentrated in vacuum to give the title compound (22.8 g, unpurified) as a colorless oil, which was used directly for the next step.

^{1}H NMR (400 MHz, $CDCl_3$) δ 5.37 (d, J = 9.0 Hz, 1H), 4.35 (d, J = 9.0 Hz, 1H), 3.74 (dd, J_1 = 3.0 Hz, J_2 = 9.0 Hz 1H), 3.69 (s, 3H), 3.74 (dd, J_1 = 3.0 Hz, J_2 = 9.0 Hz 1H), 1.40 (s, 9H), 1.11 (s, 9H).

Step 2: Synthesis of *tert*-butyl (*S*)-(3-(*tert*-butoxy)-1-hydrazinyl-1-oxopropan-2-yl)carbamate

To a solution of methyl *N*-(*tert*-butoxycarbonyl)-*O*-(*tert*-butyl)-*L*-serinate (23 g, 83.5 mmol, 1.0 equiv) in methanol (230 mL, 0.36 M) was added hydrazine monohydrate (25.1 g, 501 mmol, 6.0 equiv) at 15 °C. The mixture was stirred at 15 °C for 16 h. TLC analysis (petroleum ether/ethyl acetate = 3:1, Rf (SM) = 0.7, methanol/dichloromethane = 15:1, Rf (Prod) = 0.4) showed the starting material was consumed completely. The mixture was concentrated under reduced pressure to remove the methanol. The residue was dissolved in ethyl acetate (150 mL) and washed with aqueous sodium bicarbonate (2 × 60 mL). The combined organic phases were dried over anhydrous sodium sulfate, filtered and the filtrate was concentrated under vacuum to give the title compound (15 g, 65% yield) as a colorless oil, which was used directly for the next step.

^{1}H NMR (400 MHz, $CDCl_3$) δ 7.76 (br.s, 1H), 5.39 (br.s, 1H), 4.18 (s, 1H), 3.89 (br.s, 2H), 3.75 (dd, J_1 = 2.8 Hz, J_2 = 9.0 Hz, 1H), 3.38 (t, *J* = 8.0 Hz, 1H), 1.43 (s, 9H), 1.16 (s, 9H).

Step 3: Synthesis of *tert*-butyl ((5*S*,10*S*)-5-(2-amino-2-oxoethyl)-13,13-dimethyl-3,6,9-trioxo-1-phenyl-2,12-dioxa-4,7,8-triazatetradecan-10-yl)carbamate

To a solution of *tert*-butyl (*S*)-(3-(*tert*-butoxy)-1-hydrazinyl-1-oxopropan-2-yl)carbamate (14.4 g, 53.9 mmol, 1.1 equiv) in *N,N*-dimethylformamide (140 mL, 0.39 M) was added dicyclohexylcarbodiimide (25.3 g, 123 mmol, 2.5 equiv) and HOBt (13.3 g, 98.1 mmol, 2.0 equiv) at 0°C. The resulting mixture was stirred 0 °C for 5 min and to the mixture was added drop-wise a solution of ((benzyloxy)carbonyl)-*L*-asparagine (13.5 g, 49 mmol, 1.0 equiv, Alfa Aesar CAS# 2304-96-3) in *N,N*-dimethylformamide (80 mL) at 0 °C. The mixture was stirred at this temperature for 1 h and then allowed to warm to 15 °C and stirred at 15 °C for 16 h. The resulting mixture was filtered to remove formed solid and the filtrate was poured into ice-water (300 mL) and a precipitate formed. The mixture was filtered and the filtered cake was dried under *vacuum*. The filter cake was dissolved in *N,N*-dimethylformamide (250 mL) and poured into water (300 mL). The solid was separated out by filtration and the filtrate was dried in *vacuum* to give the title (9.6 g, unpurified) as an off-white solid. This solid contained *N,N*-dimethylformamide and urea byproduct.

^{1}H NMR (400 MHz, CD_3OD) δ 7.50-7.20 (m, 5 H), 5.12 (s, 2H), 4.63 (br. s, 1H), 4.26 (br. s, 1H), 3.62 (d, *J* = 4.5 Hz, 2H), 2.78 (dd, *J* = 15.5, 5.0 Hz, 1H), 2.64 (dd, *J* = 15.5, 8.0 Hz, 1H), 1.45 (s, 9H), 1.19 (s, 9H).

Step 4: Synthesis of *tert*-butyl ((*S*)-1-(2-(*L*-asparaginyl)hydrazinyl)-3-(*tert*-butoxy)-1-oxopropan-2-yl)carbamate

To a solution of *tert*-butyl ((5*S*,10*S*)-5-(2-amino-2-oxoethyl)-13,13-dimethyl-3,6,9-trioxo-1-phenyl-2,12-dioxa-4,7,8-triazatetradecan-10-yl)carbamate (7.0 g, 13.4 mmol, 1.00 equiv) in methanol (500 mL, 0.13 M) was added 10 wt% palladium hydroxide on carbon (3.0 g) and the mixture was stirred at 30 °C under a hydrogen atmosphere (50 psi) for 12 h. The reaction mixture was filtered through a celite pad, the filter cake was washed with methanol (3 × 150 mL), and the combined filtrate was concentrated under vacuum to give the title compound (6 g) as a purple solid which was used directly without purification in the next step.

^{1}H NMR (400 MHz, $CDCl_3$) δ 5.82-5.37 (m, 3H), 4.35-4.29 (m, 2 H), 3.79-3.71 (m, 2H), 3.48-3.44 (m, 2H), 2.74-2.70 (m, 1H), 2.01-1.89 (m, 2H), 1.46 (s, 9H), 1.22 (s, 9H).

LRMS (LCMS, ESI+) calcd. for $C_{16}H_{32}N_5O_6$ $[M+H]^+$: 390, found 390.

Step 5: Synthesis of benzyl *N*-(((*S*)-4-amino-1-(2-(*N*-(*tert*-butoxycarbonyl)-*O*-(*tert*-butyl)-*L*-seryl)hydrazinyl)-1,4-dioxobutan-2-yl)carbamoyl)-*O*-(*tert*-butyl)-*L*-threoninate

To a solution of *tert*-butyl ((*S*)-1-(2-(*L*-asparaginyl)hydrazinyl)-3-(*tert*-butoxy)-1-oxopropan-2-yl)carbamate (7.7 g, 19.8 mmol, 1.0 equiv) in anhydrous dichloromethane (70 mL, 0.28 M) was added a solution of benzyl *O*-(*tert*-butyl)-*N*-(1*H*-imidazole-1-carbonyl)-*L*-threoninate (6.82 g, 19.0 mmol, 0.96 equiv) in anhydrous dichloromethane (30 mL) at 0 °C, then the mixture was stirred at 15 °C for 12 h. The reaction mixture was concentrated under vacuum and the residue was purified by preparative-HPLC (Column Daiso 250 × 50 mm, 10 µm, eluting with 35% to 65% MeCN in water (+0.1% TFA) over 20 minutes, followed by 100% MeCN in water (+0.1% TFA) for 15 minutes at a flow rate of 80 mL/min. The sample was loaded onto the column over 16 injections. The desired compound (1.4 g, 10% yield) was obtained as a light yellow solid.

^{1}H NMR (400 MHz, $CDCl_3$) δ 7.40-7.30 (m, 5H), 6.88-6.86 (m, 1H), 6.75 (br.s, 1H), 6.68 (br.s, 1H), 6.01 (br.s, 1H), 5.47 (d, *J* = 6.0 Hz, 1H), 5.17 (d, *J* = 12.0 Hz, 1H), 5.07-5.03 (m, 1H), 4.92-4.89 (m, 1H), 4.54 (d, *J* = 9.0 Hz, 1H), 4.27 (br.s, 1H), 4.18-4.15 (m, 1H), 3.75-3.73 (m, 1H), 3.36 (t, *J* = 8.5 Hz, 1H), 3.10 (t, *J* = 13.5 Hz, 1H), 2.59 (dd, J_1= 15.5 Hz, J_2= 4.0 Hz, 1H), 1.43 (s, 9H), 1.21 (s, 9H), 1.17 (d, *J* = 6.4 Hz, 3H), 1.06 (s, 9H).

LRMS (LCMS, ESI+) calcd. for $C_{32}H_{53}N_6O_{10}$ $[M+H]^+$: 681, found 681.

Step 6: Synthesis of *N*-(((*S*)-4-amino-1-(2-(*N*-(*tert*-butoxycarbonyl)-*O*-(*tert*-butyl)-*L*-seryl)hydrazinyl)-1,4-dioxobutan-2-yl)carbamoyl)-*O*-(*tert*-butyl)-*L*-threonine

To a solution of benzyl *N*-(((*S*)-4-amino-1-(2-(*N*-(*tert*-butoxycarbonyl)-*O*-(*tert*-butyl)-*L*-seryl)hydrazinyl)-1,4-dioxobutan-2-yl)carbamoyl)-*O*-(*tert*-butyl)-*L*-threoninate (1.4 g, 2.37 mmol, 1.0 equiv) in methanol (50 mL, 0.05 M) was added 10 wt% palladium on carbon (700 mg) and the mixture was stirred at 30 °C under a hydrogen atmosphere (50 psi) for 3 h. The reaction mixture was filtered through a pad of celite, the filter cake was washed with methanol (3 × 50 mL) and the combined filtrate was concentrated under vacuum to afford the unpurified solid. The resulting solid was purified by preparative-HPLC (Instrument: Gilson 281 semi-preparative HPLC system) using a gradient of 65:35 to 35:65 H_2O:MeCN (+0.075% TFA) over 10 minutes, flushing with 100% MeCN for 2 minutes after the run. The column used was a Boston Green ODS 150 × 30 mm, 5 µm particle size, with a flow rate of 25 mL/min and monitoring at 220 and 254 nm wavelengths. The title compound (710 mg, 58% yield) was obtained as a white solid.

^{1}H NMR (400 MHz, d_6-DMSO) δ 9.92 (br.s, 1H), 9.80 (br.s, 1H), 6.86 (br.s, 1H), 6.75 (br.s, 1H), 6.57 (d, *J* = 8.5 Hz, 1H), 6.18 (d, *J* = 9.0 Hz, 1H), 4.45 (br.s, 1H), 4.07-4.04 (m, 4H), 3.48-3.44 (m, 1H), 3.39-3.35 (m, 1H), 2.42-2.41(m, 1H), 2.34-2.28 (m, 1H), 1.35 (s, 9H), 1.09 (s, 9H), 1.07 (s, 9H), 1.03 (d, *J* = 6.5 Hz, 3H).

LRMS (LCMS, ESI+) calcd. for $C_{25}H_{47}N_6O_{10}$ $[M+H]^+$: 591, found 591.

Step 7: Synthesis of (((*S*)-1-(2-(*L*-seryl)hydrazinyl)-4-amino-1,4-dioxobutan-2-yl)carbamoyl)-*L*-threonine trifluoracetate

To a solution of *N*-(((*S*)-4-amino-1-(2-(*N*-(*tert*-butoxycarbonyl)-*O*-(*tert*-butyl)-*L*-seryl)hydrazinyl)-1,4-dioxobutan-2-yl)carbamoyl)-*O*-(*tert*-butyl)-*L*-threonine (700 mg, 1.19 mmol, 1.0 equiv) in dichloromethane (30 mL) was added trifluoroacetic acid (30 mL) and the resulting mixture was stirred at 15 °C for 12 h. The reaction mixture was concentrated under vacuum to afford a residue. The resulting

residue was purified by preparative-HPLC (Instrument: Gilson 281 semi-preparative HPLC system) using a gradient of 5:95 to 10:90 H_2O:MeCN (+0.075% TFA) over 12 minutes, flushing with 100% MeCN for 7 minutes after the run. The column used was an Atlantis Hilic Silica 150 × 19 mm, 5 µm particle size, with a flow rate of 25 mL/min and monitoring at 220 and 254 nm wavelengths. The title compound (trifluoroacetate salt, 102 mg, 23 % yield) was obtained as a white solid.

^{1}H NMR (400 MHz, D_2O) δ 4.70-4.65 (m, 1H), 4.34-4.30 (m, 1H), 4.25-4.22 (m, 2H), 4.02-3.99 (m, 2H), 2.92-2.75 (m, 2H), 1.20 (d, *J* = 2.8 Hz, 3H).

LRMS (LCMS, ESI+) calcd. for $C_{12}H_{23}N_6O_8$ $[M+H]^+$: 379, found 379.

4b. Synthesis of Compound **2**

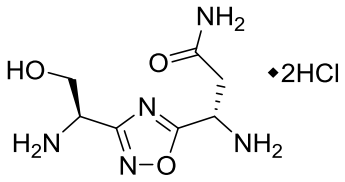

Compound **2**

This compound was described in WO 2015/033299, Example 1 and identical chemistry was used herein to prepare this material at Santai Labs. The characterization data for the final compound is shown below. Nuclear Magnetic Resonance (NMR) analysis was conducted using a Bruker 400 MHz spectrometer with an appropriate deuterated solvent. LCMS analysis was conducted using a Shimadzu LC-ATvp with an API 150EX detector using an Agilent Zorbax Eclipse IDB-C18 3.5 µM, 2.1 × 50 mm column, eluting with 95:5 to 20:80 H_2O:MeCN + 0.02% formic acid over 4 minutes.

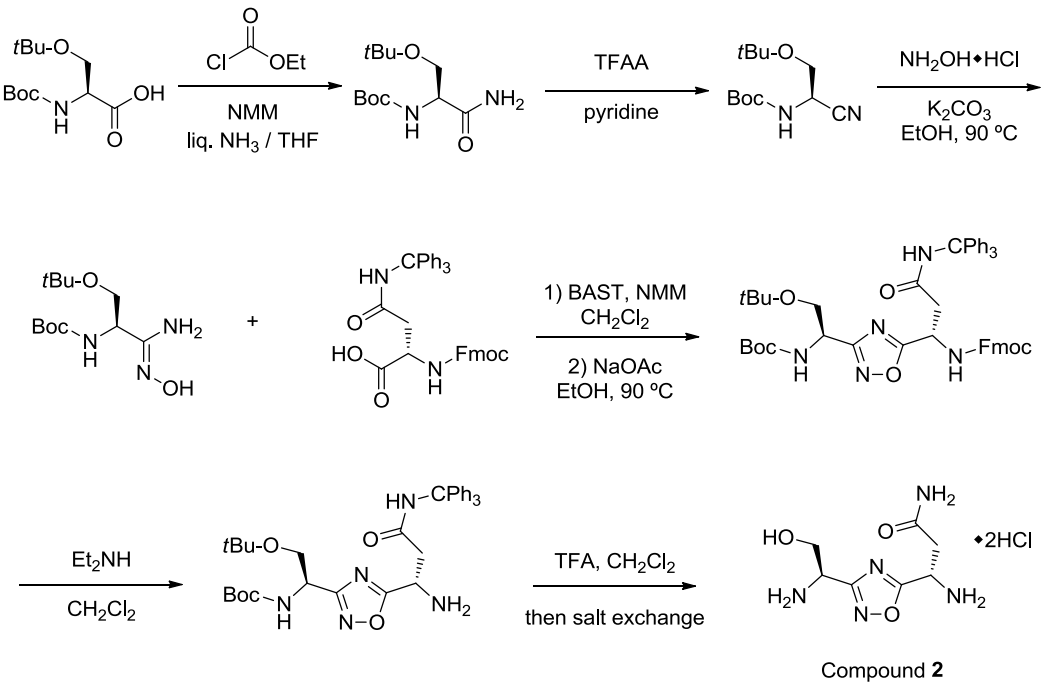

Compound **2**

^{1}H NMR (400 MHz, CD_3OD) δ 5.21-5.19 (bs, 1H), 4.07 (bs, 1H), 4.03-4.00 (m, 2H), 3.23-3.22 (m, 2H).

^{13}C NMR (100 MHz, D_2O) δ 176.36, 172.26, 166.06, 59.89, 49.20, 44.86, 34.66.

LRMS (LCMS, ESI+) calcd. for $C_7H_{13}N_5NaO_3$ $[M+Na]^+$: 238, found 238.

4c. Synthesis of Compound **3**

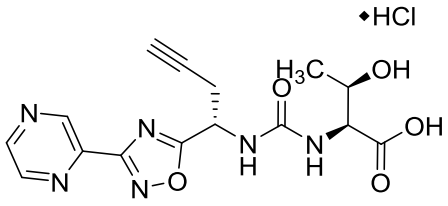

Compound **3**

This compound was described in WO 2016/142886, Example 32 and identical chemistry was used herein to prepare this material at Santai Labs. The characterization data for the final compound is shown below. Nuclear Magnetic Resonance (NMR) analysis was conducted using a Bruker 400 MHz spectrometer with an appropriate deuterated solvent. LCMS analysis was conducted using a Shimadzu LC-ATvp with an API 150EX detector using an Agilent Zorbax Eclipse IDB-C18 3.5 µM, 2.1 × 50 mm column, eluting with 95:5 to 20:80 H_2O:MeCN + 0.02% formic acid over 4 minutes.

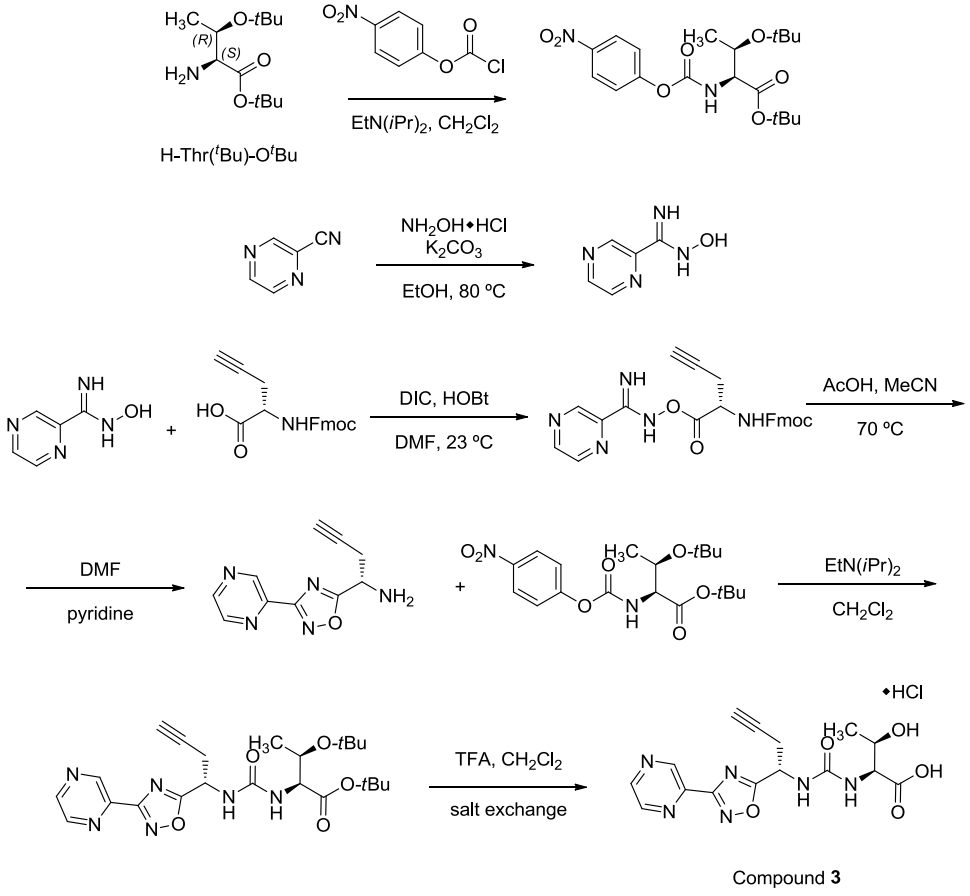

^{1}H NMR (400 MHz, CD_3OD) δ 9.33 (s, 1H), 8.79 (d, *J* = 7.0 Hz, 2H), 5.39 (t, *J* = 6.0 Hz, 1H), 4.31 (d, *J* = 7.0 Hz), 4.25 (s, 1H), 2.98 (m, 2H), 2.45 (s, 1H), 1.21 (d, *J* = 6.0 Hz).

LRMS (LCMS, ESI+) calcd. for $C_{15}H_{17}N_6O_5$ $[M+H]^+$: 361, found 361.

4d. Synthesis of Compound **4**

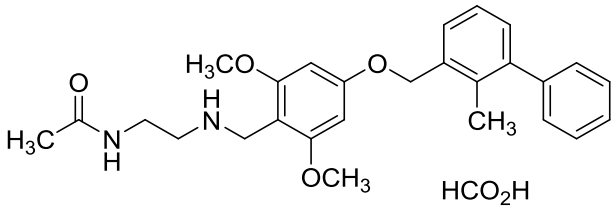

Compound **4**

This compound was described in WO 2015/034820 and similar chemistry was used herein to prepare this material at Inception Sciences Vancouver. Nuclear Magnetic Resonance (NMR) analysis was conducted using a Varian Mercury 300 MHz spectrometer with an appropriate deuterated solvent. LCMS analysis was conducted using a Waters Acquity UPLC with a QDA MS detector using a Waters C18 BEH 1.7 µM, 2.1 × 50 mm column, eluting with 95:5 to 0:100 H_2O:MeCN + 0.1% formic acid at a flow rate of 0.6 mL/min over 3.5 minutes. The QDA MS detector was set up to scan under both positive and negative mode ions ranging from 100-1200 Daltons.

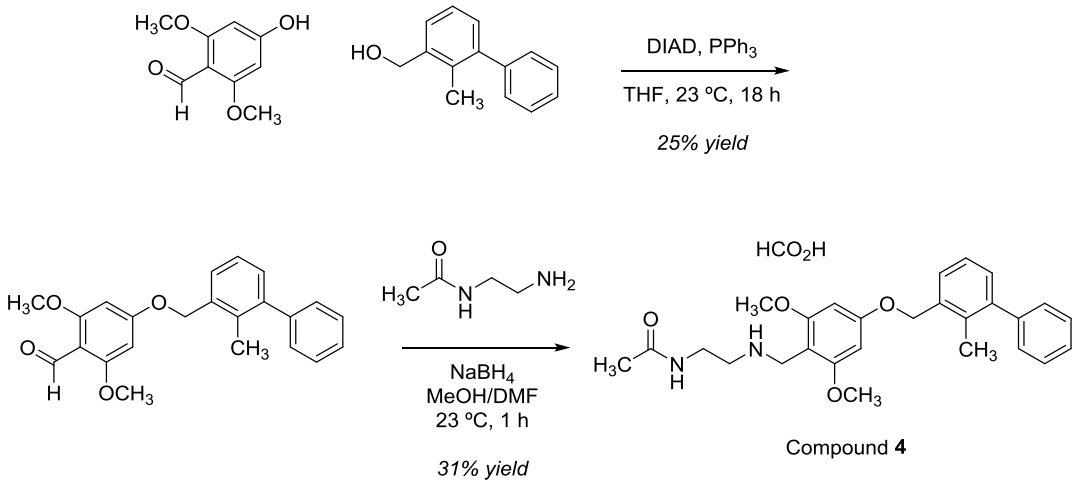

Compound **4**

Step 1: Synthesis of 2,6-dimethoxy-4-((2-methyl-[1,1'-biphenyl]-3-yl)methoxy)benzaldehyde

Into a 20 mL sample vial equipped with a magnetic stir bar and under N_2 was added 3-hydroxymethyl 2-methylbiphenyl (1.08 g, 5.49 mmol, 1.0 equiv, TCI CAS# 76350-90-8), 2,6-dimethoxy-4-hydroxybenzaldehyde (1.00 g, 5.49 mmol, 1.0 equiv, Aldrich CAS# 22080-96-2), triphenylphosphine (2.16 g, 8.23 mmol, 1.5 equiv) and THF (2.0 mL, 2.8 M). The solution was treated with drop-wise addition of di-*iso*-propyl azodicarboxylate (1.62 mL, 8.23 mmol, 1.5 equiv) over 10 minutes and the red-orange solution was stirred at 23 ˚C for 18 h overnight. The reaction mixture was loaded directly onto a 20 g silica gel pre-cartridge and dried. Purification by column chromatography through silica gel (80 g) on an

automated Teledyne ISCO Rf200, eluting with 80:20 to 20:80 hexanes:EtOAc as a gradient over 25 minutes, collecting all peaks. The desired product was isolated, concentrated and dried under vacuum to afford an off-white solid (535 mg, 27% yield).

^{1}H NMR (300 MHz, $CDCl_3$) δ 10.37 (s, 1H), 7.41-7.26 (m, 8H), 6.20 (s, 2H), 5.16 (s, 2H), 3.89 (s, 6H), 2.27 (s, 3H).

LRMS (LCMS, ESI+) calcd. for $C_{23}H_{23}O_4$ $[M+H]^+$: 363, found 363.

Step 2: Synthesis of *N*-(2-((2,6-dimethoxy-4-((2-methyl-[1,1'-biphenyl]-3-yl)methoxy)benzyl)amino)ethyl) acetamide

Into a 20 mL sample vial equipped with a magnetic stir bar and under N_2 was added 2,6-dimethoxy-4-((2-methyl-[1,1'-biphenyl]-3-yl)methoxy)benzaldehyde (250 mg, 0.69 mmol, 1.0 equiv), DMF (2 mL, 0.35 M), acetic acid (40 µL, 0.69 mmol, 1.0 equiv) and *N*-(2-amino)ethyl acetamide (211 mg, 2.07 mmol, 3.0 equiv). The yellow-orange mixture was heated to 40 ˚C for 1 h and then cooled to room temperature. The solution was treated with $NaBH_4$ (76 mg, 2.07 mmol, 3.0 equiv) added portion-wise over 10 minutes and the mixture was stirred at 23 ˚C for 1 h. LCMS analysis after this time reveals product formation. The mixture was cooled to 0 ˚C and quenched with drop-wise addition of water (3 mL) and concentrated under reduced pressure. The unpurified reaction mixture was suspended in MeOH and loaded onto a 5 g C18 pre-cartridge and dried. Purification by reverse-phase column chromatography through C18 media (26 g) on an automated Teledyne ISCO Rf200, eluting with 100:0 to 40:60 H_2O:MeCN + 0.1% HCO_2H as a gradient over 20 minutes afforded the formate salt of the desired compound as a clear film (106 mg, 31% yield).

^{1}H NMR (300 MHz, $CDCl_3$) δ 8.47 (br.s, 1H), 7.42-7.26 (m, 8H), 6.23 (s, 2H), 5.08 (s, 2H), 4.13 (br.s, 2H), 3.83 (s, 6H), 3.49 (br.s, 2H), 2.98 (br.s, 2H), 2.26 (3H, s), 1.96 (3H, s).

LRMS (LCMS, ESI+) calcd. for $C_{27}H_3N_2O_4$ $[M+H]^+$: 449, found 449.

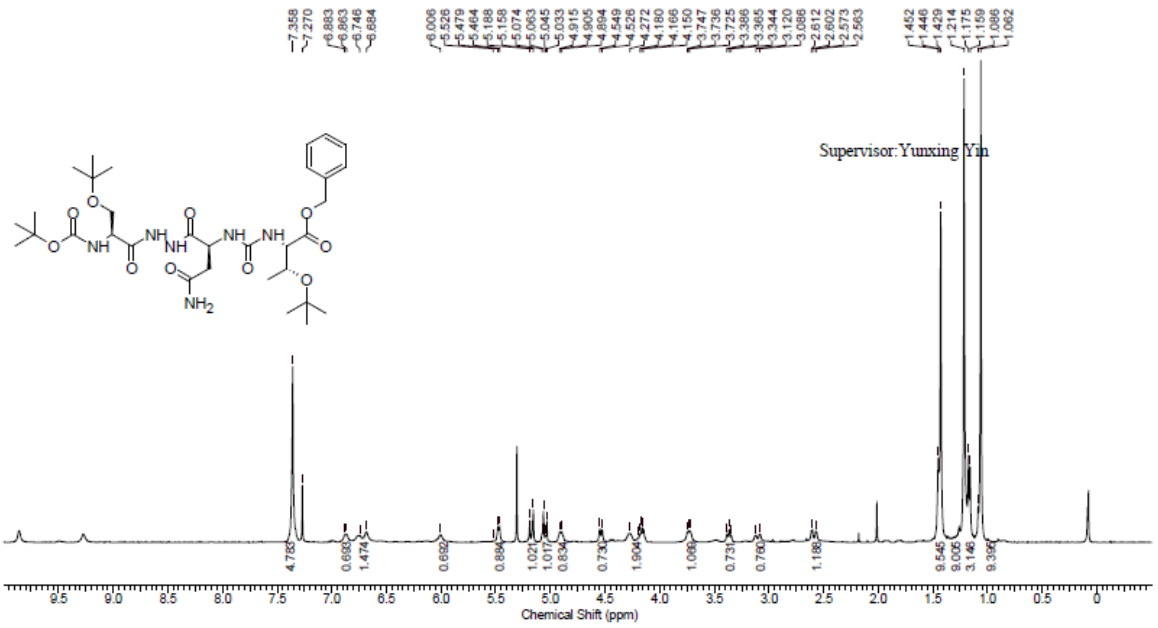

Figure S9. ^{1}H NMR spectrum for fully protected precursor leading to compound **1** in $CDCl_3$.

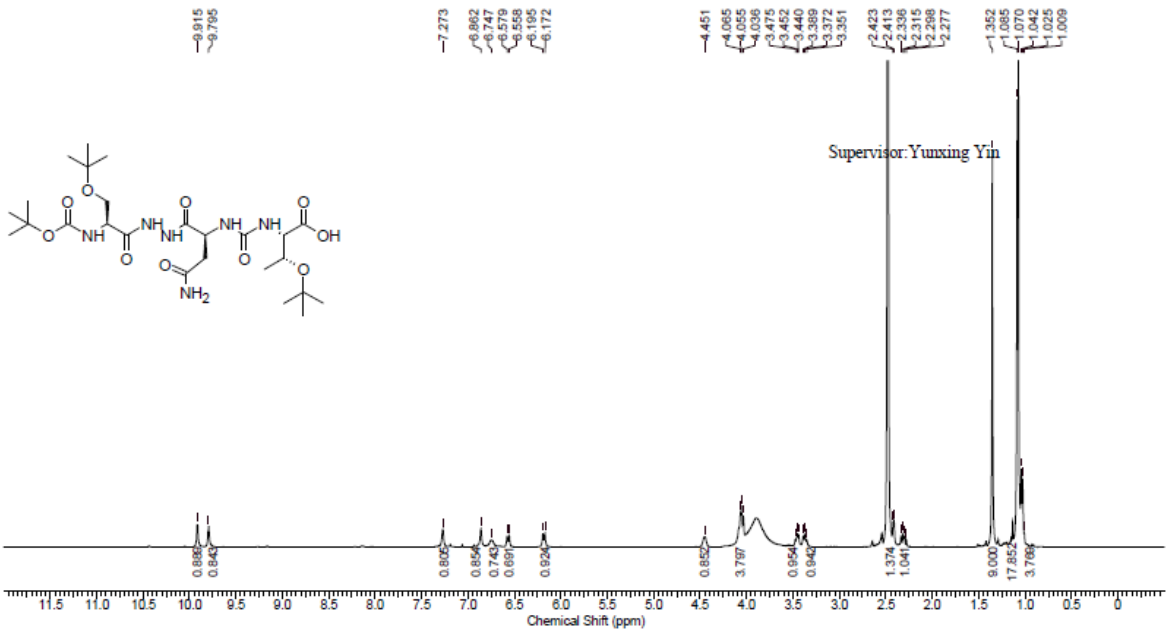

Figure S10. ^{1}H NMR spectrum for penultimate intermediate leading to compound **1** in d_6-DMSO.

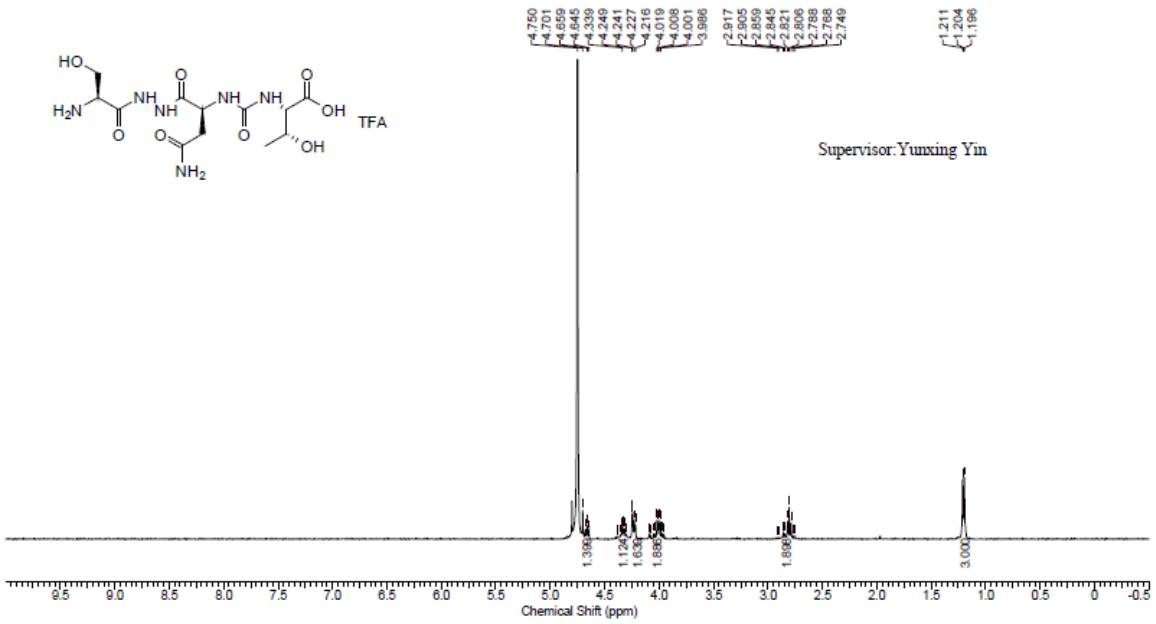

Figure S11. ^{1}H NMR spectrum for compound **1** in D_2O.

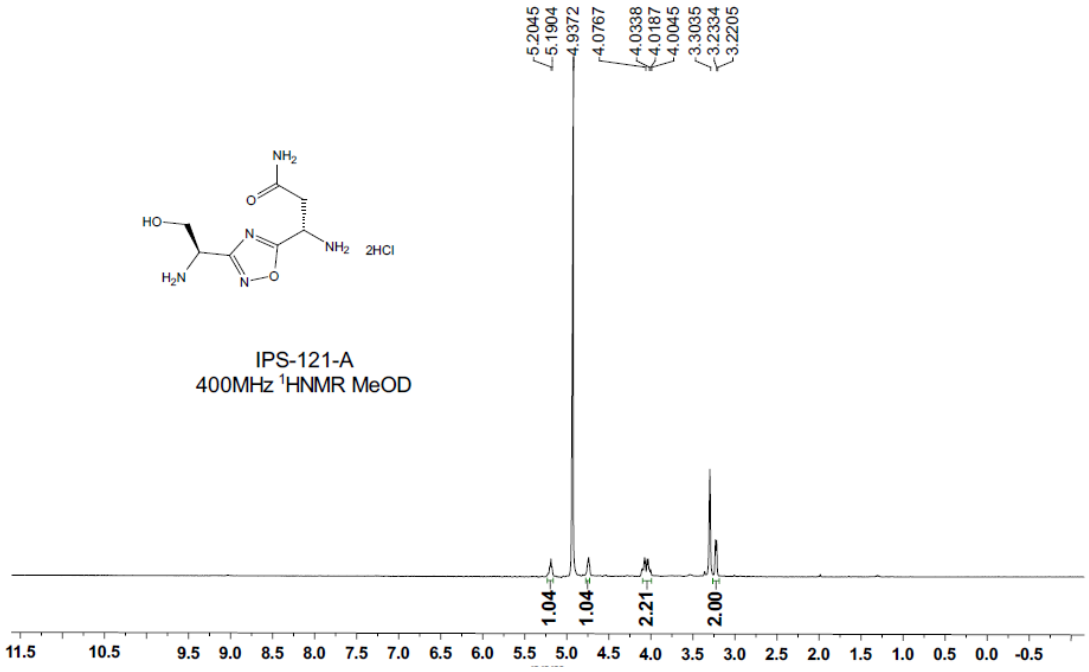

Figure S12. ^{1}H NMR spectrum for compound **2** in CD_3OD.

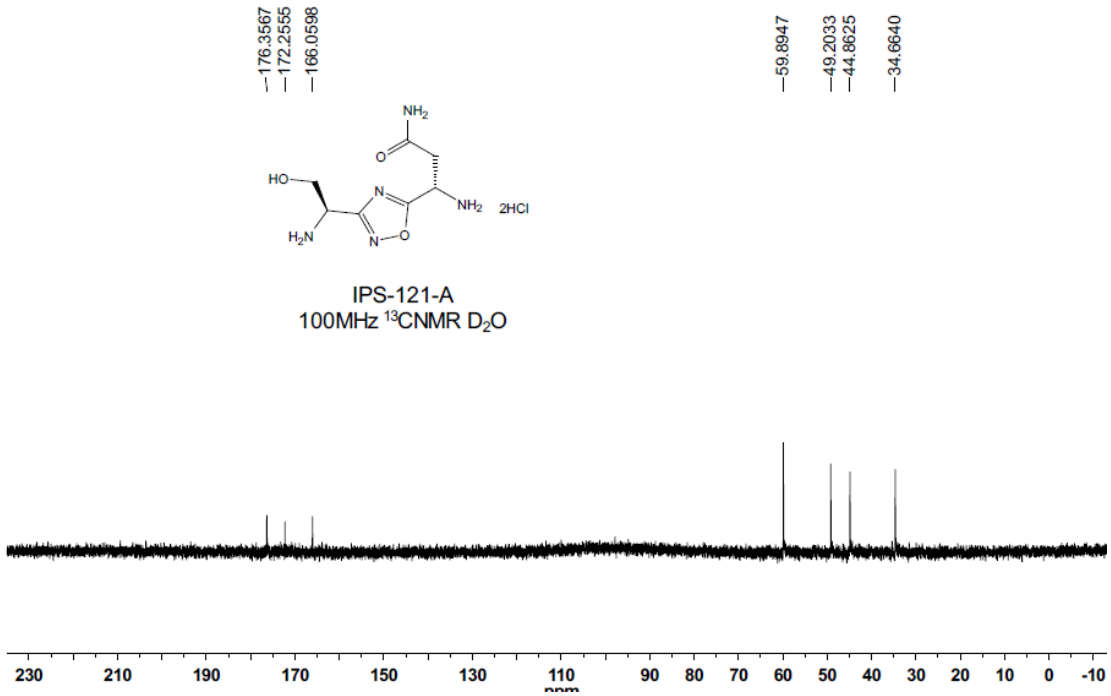

Figure S13. ^{13}C NMR spectrum for compound **2** in D_2O.

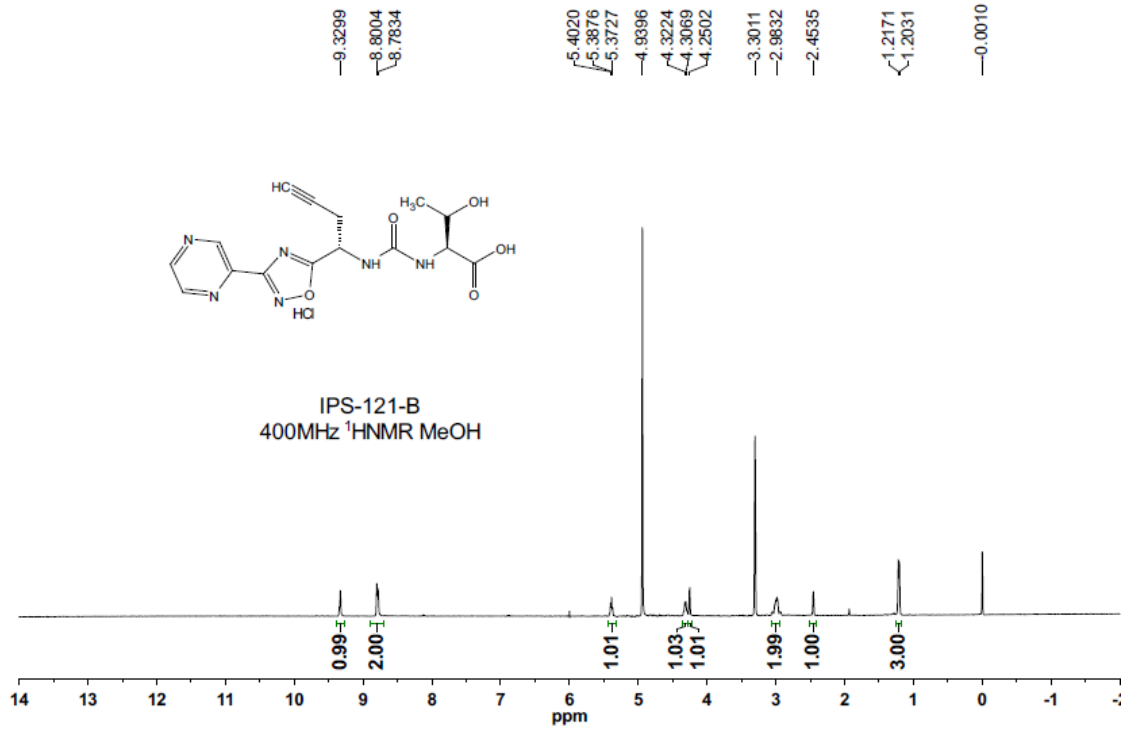

Figure S14. ^{1}H NMR spectrum for compound **3** in CD_3OD.

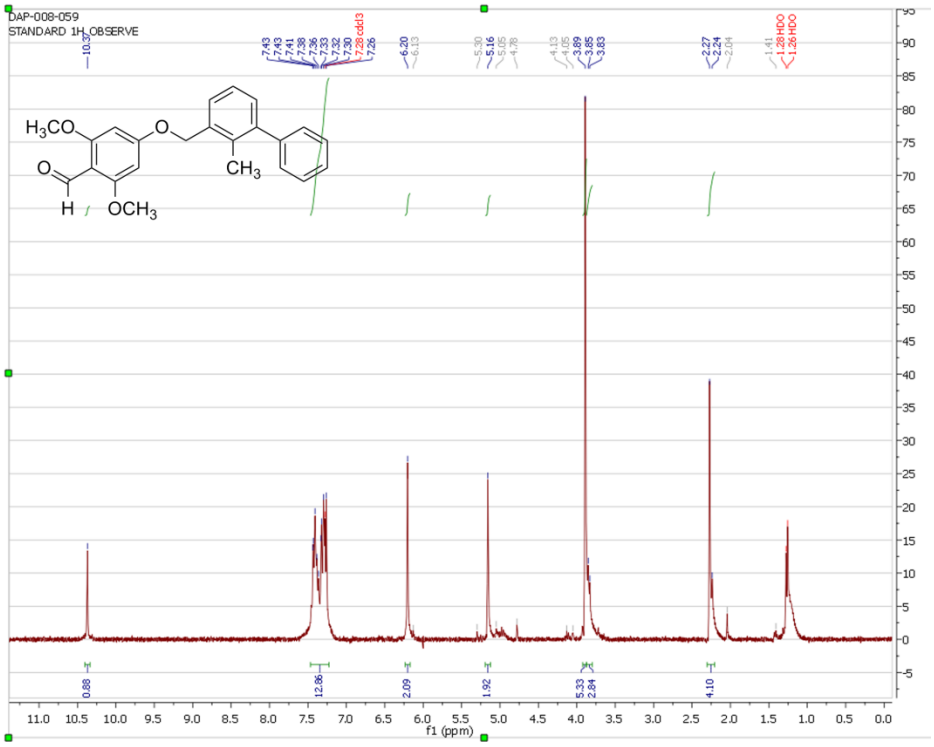

Figure S15. ^{1}H NMR spectrum for 2,6-dimethoxy-4-((2-methyl-[1,1'-biphenyl]-3-yl)methoxy) benzaldehyde (aldehyde intermediate en route to compound **4**) in $CDCl_3$.

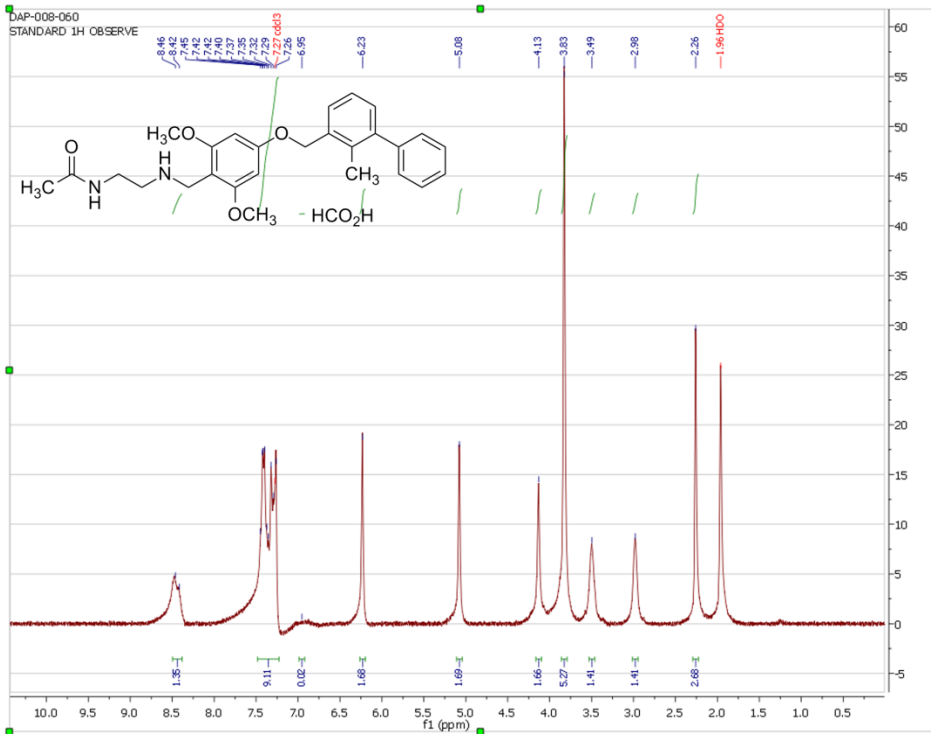

Figure S16. ^{1}H NMR spectrum for compound **4** in $CDCl_3$.